Geophys. J. Int. (1999) **139,** 227–247

A Maastrichtian palaeomagnetic pole for the Pacific plate from a skewness analysis of marine magnetic anomaly 32

Katerina E. Petronotis[1] and Richard G. Gordon[2]

[1] *Ocean Drilling Program, Texas A&M University, College Station,* TX 77845-9547, *USA*
[2] *Department of Geology & Geophysics, Rice University, Houston,* TX 77005-1892, *USA. E-mail: rgg@geophysics.rice.edu*

Accepted 1999 April 13. Received 1999 April 13; in original form 1998 August 21

SUMMARY

The asymmetry (skewness) of marine magnetic anomaly 32 (72.1–73.3 Ma) on the Pacific plate has been analysed in order to estimate a new palaeomagnetic pole. Apparent effective remanent inclinations of the seafloor magnetization were calculated from skewness estimates of 108 crossings of anomaly 32 distributed over the entire Pacific plate and spanning a great-circle distance of $\sim$12 000 km. The data were inverted to obtain a palaeomagnetic pole at 72.1°N, 26.8°E with a 95 per cent confidence ellipse having a 4.0° major semi-axis oriented 98° clockwise of north and a 1.8° minor semi-axis; the anomalous skewness is $14.2° \pm 3.7°$. The possible dependence of anomalous skewness on spreading rate was investigated with two empirical models and found to have a negligible effect on our palaeopole analysis over the range of relevant spreading half-rates, $\sim$25 to $\sim$90 mm yr^{-1}. The new pole is consistent with the northward motion for the Pacific plate indicated by coeval palaeocolatitude and palaeoequatorial data, but differs significantly from, and lies to the northeast of, coeval seamount poles. We attribute the difference to unmodelled errors in the seamount poles, mainly in the declinations. Comparison with the northward motion inferred from dated volcanoes along the Hawaiian–Emperor seamount chain indicates 13° of southward motion of the Hawaiian hotspot since 73 Ma. When the pole is reconstructed with the Pacific plate relative to the Pacific hotspots, it differs by 14°–18° from the position of the pole relative to the Indo–Atlantic hotspots. This has several possible explanations including bias in one or more of the palaeomagnetic poles, motion between the Pacific and Indo–Atlantic hotspots, and errors in plate reconstructions relative to the hotspots.

Key words: anomalous skewness, apparent polar wander, hotspots, marine magnetic anomalies, Pacific plate, palaeomagnetic poles.

INTRODUCTION

Skewness data obtained from marine magnetic anomalies (Schouten & McCamy 1972; Schouten & Cande 1976) have the potential to improve the accuracy and age resolution of the apparent polar wander (APW) path of the Pacific plate by providing palaeomagnetic poles with well-known ages and by complementing other oceanic palaeomagnetic data such as seamount poles and palaeocolatitudes determined from the palaeomagnetic study of azimuthally unoriented core samples. New palaeomagnetic poles have important implications for plate reconstruction tests, for the motion of the palaeomagnetic axis relative to the hotspots, and for testing whether hotspots are stationary relative to one another.

Some early work applying the skewness method was limited by the discovery of an apparently systematic error known as anomalous skewness (Weissel & Hayes 1972; Cande & Kent 1976). Anomalous skewness could be isolated for anomalies with counterparts across a mid-ocean ridge (Cande 1976; Cande & Kristoffersen 1977; Cande 1978), but was much harder to estimate for anomalies with counterparts that have been subducted, as is the case for most counterparts of anomalies on the Pacific plate (Cande 1976). We previously presented a solution to this problem by simultaneously estimating anomalous skewness and a best-fitting palaeomagnetic pole from skewness data from a single plate (Petronotis *et al.* 1992), and applied it to 132 crossings of anomaly 25r on the Pacific plate (Petronotis *et al.* 1994).

Here we determine a new Maastrichtian palaeomagnetic pole with usefully compact confidence limits from an analysis of the skewness of magnetic anomaly 32 (Fig. 1) [72.1–73.3 Ma on the timescale of Cande & Kent (1992), which is used

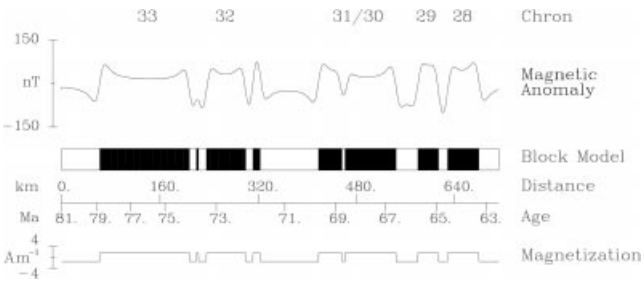

Figure 1. Synthetic magnetic profile of the anomaly 28–33 sequence. The lower curve gives the range of magnetization values used to construct this particular example. The block model illustrates the assumption of vertical boundaries between regions of seafloor with alternating polarities that was used to calculate the magnetic anomaly. The chron ages are based on the timescale of Cande & Kent (1992).

throughout this paper]. We analysed the skewness of 108 crossings of anomaly 32 over seafloor formed by Pacific–Kula, Pacific–Farallon, Pacific–Aluk, Pacific–Bellingshausen, and Pacific–Antarctic spreading.

METHODS

Relation between skewness and apparent effective inclination

The first step in a palaeomagnetic analysis of marine magnetic anomalies is to estimate the skewness of a magnetic anomaly crossing. The skewness depends on the direction of remanent magnetization of the seafloor, the present direction of the Earth's magnetic field, and the azimuth of the magnetic anomaly lineation. The skewness is described by a phase parameter, $\Delta\theta$, which quantifies how much the shape of an observed anomaly differs from the shape expected above seafloor formed and observed in a downward vertical magnetic field. The ideal or reference shape is obtained from synthetic magnetic profiles that are generated assuming vertical polarity boundaries, vertical downward ambient magnetic field and remanent magnetization, magnetization intensities of 0.002–0.02 emu cc^{-1} (2 to 10 A m^{-1}), transition widths of 12–16 km, and spreading rates appropriate for the plate pairs being considered (Fig. 1). Details of these parameters and how we estimate $\Delta\theta$ have been presented in our earlier papers (Petronotis & Gordon 1989; Petronotis *et al.* 1992, 1994).

The next step is the calculation of the *apparent* effective remanent inclination, e_a, of the seafloor from the experimentally determined phase shift $\Delta\theta$ by

$$e_a = -\Delta\theta - e + 180^\circ \quad (1)$$

(Schouten & McCamy 1972; Schouten & Cande 1976; Petronotis *et al.* 1992), where e, the ambient effective inclination at the site, is obtained from

$$e = \tan^{-1}(\tan I/\sin \alpha), \quad (2)$$

where $\alpha = A - D$, I and D are the inclination and declination of the ambient geomagnetic field at the site, which we estimate from the International Geomagnetic Reference Field, and A, the azimuth of the magnetic lineation at the site, is taken to be the strike direction that is 90° clockwise of the direction in which the seafloor becomes younger.

The apparent effective remanent inclination gives a biased estimate of the true effective remanent inclination. This bias is termed anomalous skewness (Cande 1976; Petronotis *et al.* 1992). Anomalous skewness is a simple empirical parametrization of differences between the simple magnetization models with vertical boundaries used in our studies to date and the true processes and geometry of seafloor magnetization.

Model estimation by least-squares inversion

The effective remanent inclination can be predicted by a function that depends on the latitude and longitude of the site, the latitude and longitude of the palaeomagnetic pole, and the azimuth of the magnetic lineation (Schouten & Cande 1976; Gordon & Cox 1980; Petronotis *et al.* 1992). We assume that

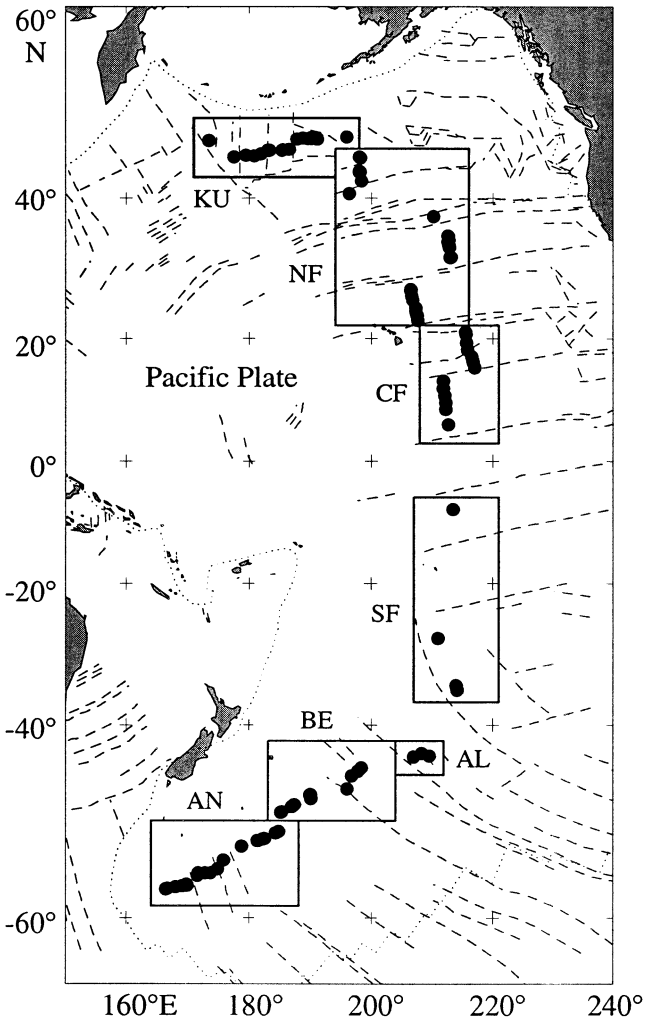

Figure 2. Map of the Pacific basin showing the locations of crossings of anomaly 32. Dotted lines show plate boundaries. Thin dashed lines show the locations of fracture zones, pseudo-faults, similar seafloor features, and the Pacific–Farallon–Aluk triple junction trace. Seven subregions of the Pacific plate are indicated and labelled as follows: KU, Pacific–Kula; NF, northern Pacific–Farallon; CF, central Pacific–Farallon; SF, southern Pacific–Farallon; AL, Pacific–Aluk; BE, Pacific–Bellingshausen; AN, Pacific–Antarctic. Detailed maps for each subregion with identifications of each crossing are available at the following URL: http://terra.rice.edu/department/faculty/gordon/skewness/c32

anomalous skewness is the same at all sites (Petronotis *et al.* 1992). Since anomalous skewness and the coordinates of the pole are unknown, we use trial values for these parameters to calculate a model apparent effective inclination at each site:

$$e_m = e_r - \theta_a, \tag{3}$$

where θ_a is the anomalous skewness and e_r is the effective remanent inclination, which is given by $e_r = \tan^{-1}(\tan I_r / \sin \alpha_r)$, in which $\alpha_r = A - D_r$. The model apparent effective inclinations (e_m) are then compared with the observations; that is the apparent effective remanent inclinations (e_a). The method for finding the least-squares estimates of pole latitude, pole longitude, and anomalous skewness, as well as the method for estimating the information contribution ('importance') of each datum, are described by Petronotis *et al.* (1992).

This formulation neglects the possible dependence of anomalous skewness on spreading rate or on depth or thickness of the magnetic layer (Cande 1978; Roest *et al.* 1992; Dyment *et al.* 1994). Our earlier estimation of a palaeomagnetic pole for chron 25r showed that when the range of spreading rates is small, the variation of anomalous skewness has a negligible effect on the pole (Petronotis *et al.* 1994). In a later section we investigate the different ways in which anomalous skewness can depend on spreading rate and how these can affect the palaeomagnetic pole for chron 32.

Confidence limits

Confidence limits on the best-fitting pole and anomalous skewness are propagated from the uncertainties assigned to the apparent effective inclinations by two alternative methods: constant-chi-square boundaries and linear propagation of errors. The latter method approximates the constant-chi-square confidence region of the palaeomagnetic pole well only if the data

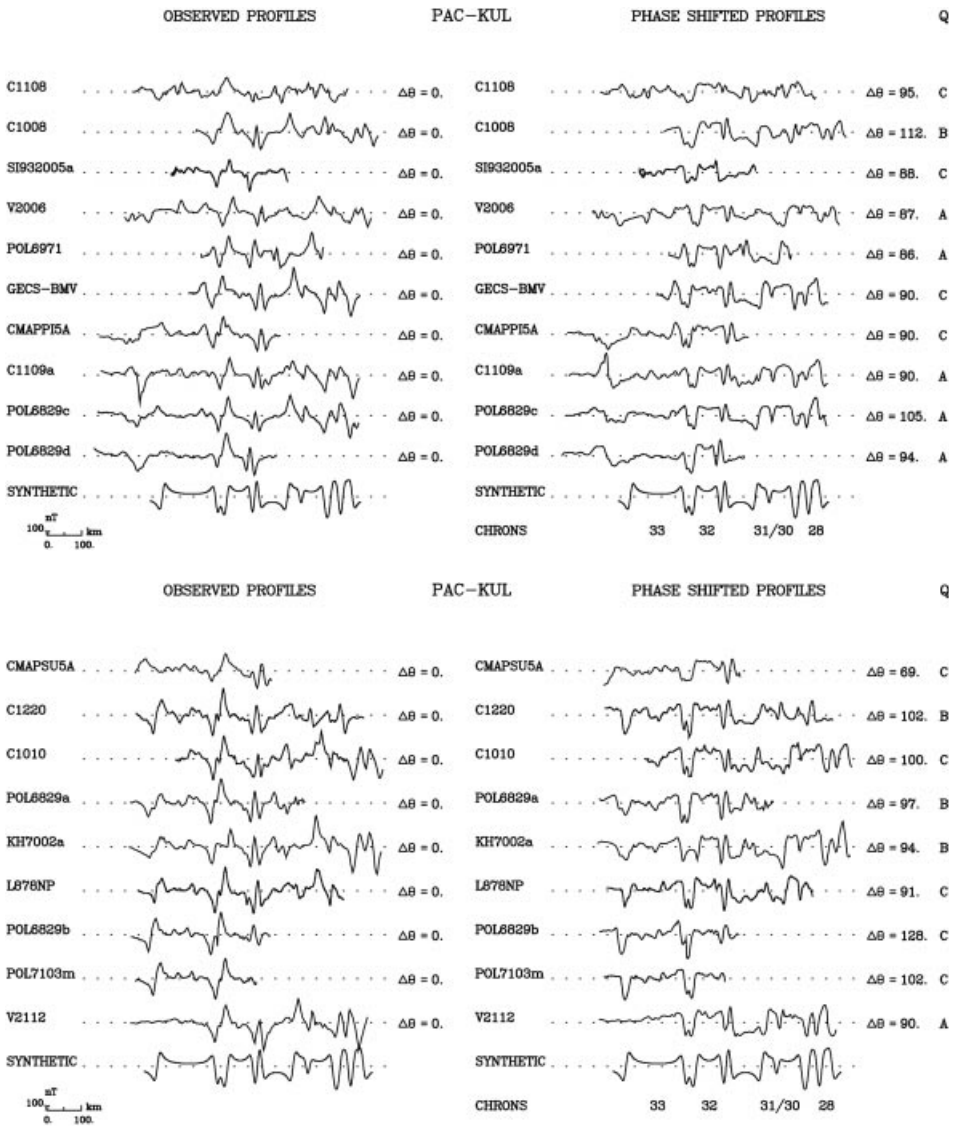

Figure 3. Profiles obtained over seafloor produced by Pacific–Kula seafloor spreading. (Left panels) Original profiles projected perpendicular to lineation strike. (Right panels) Phase-shifted profiles. The phase shift ($\Delta\theta$) that best deskews anomaly 32 and the quality (Q) of the anomaly are shown on the right side of the deskewed profile. The synthetic profiles show the sequence from anomaly 33n (on the left) to anomaly 28n (on the right). The synthetics show the same sequence on all such plots unless otherwise indicated. The east longitude of the profiles increases from the top to the bottom of the figure.

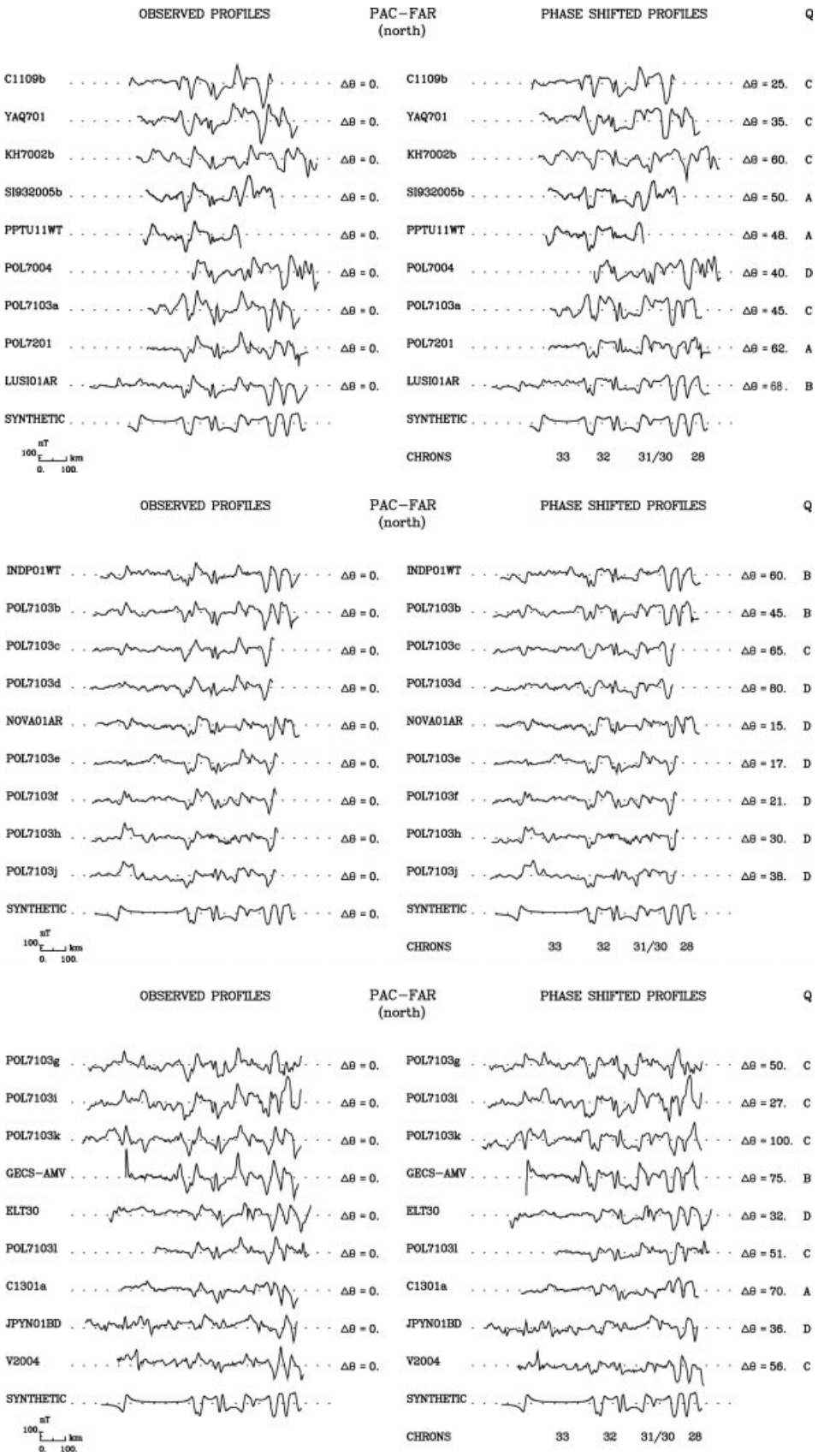

Figure 4. Profiles obtained over seafloor between 45°N and 22°N produced by Pacific–Farallon seafloor spreading. The north latitude of the profiles decreases from the top to the bottom of the figure.

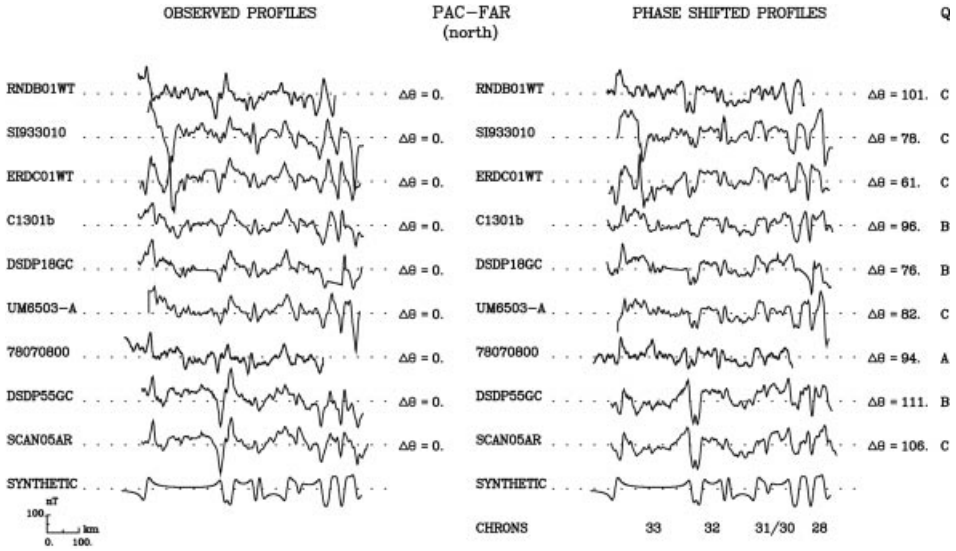

Figure 4. (*Continued.*)

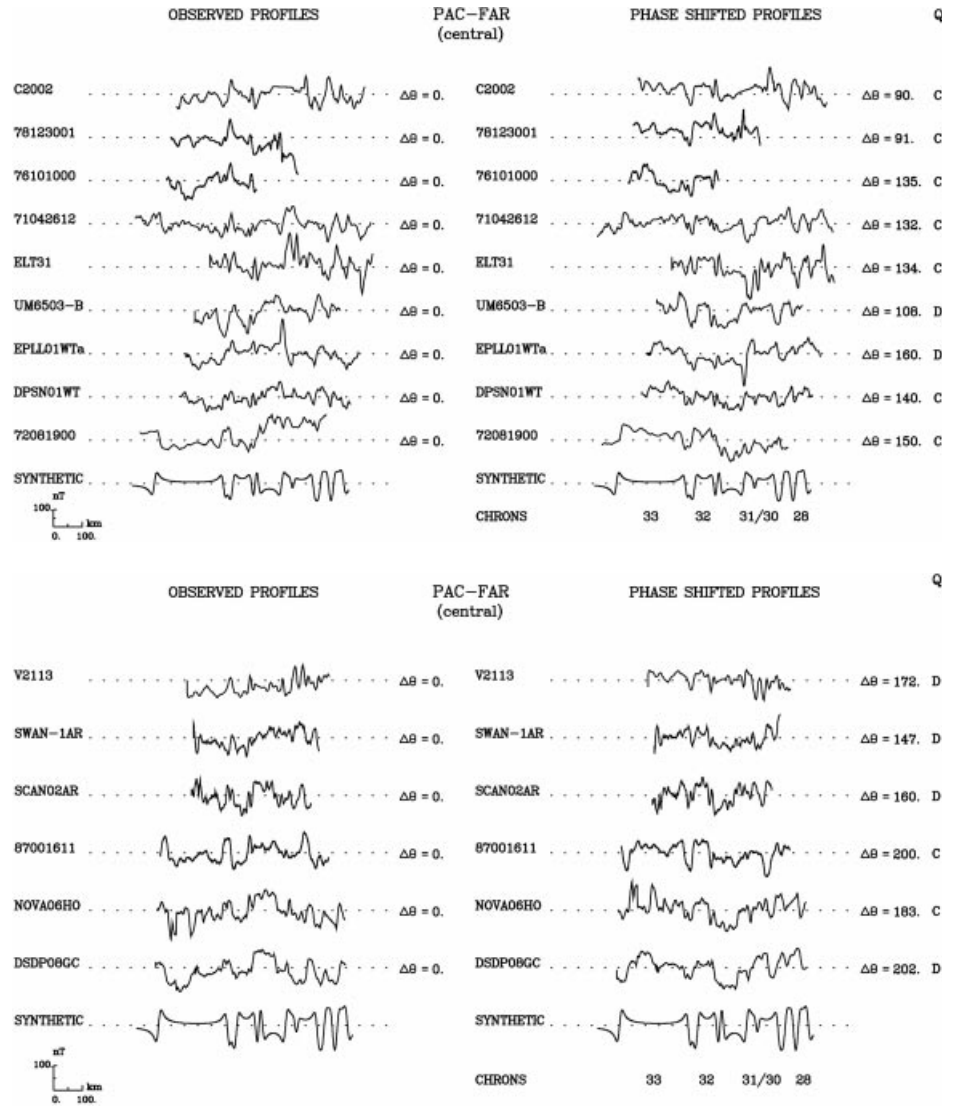

Figure 5. Profiles obtained over seafloor between 22°N and 6°N produced by Pacific–Farallon seafloor spreading. The north latitude of the profiles decreases from the top to the bottom of the figure.

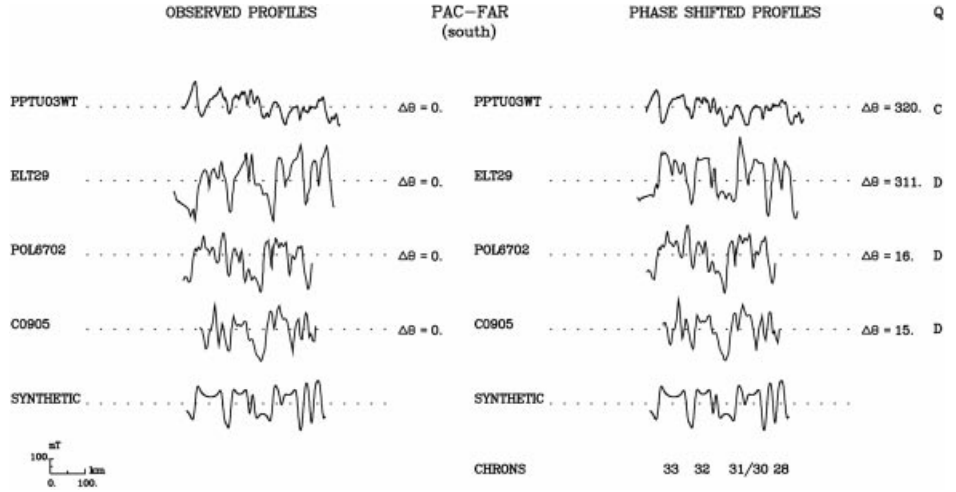

Figure 6. Profiles obtained over seafloor between 8°S and 35°S produced by Pacific–Farallon seafloor spreading. The south latitude of the profiles increases from the top to the bottom of the figure.

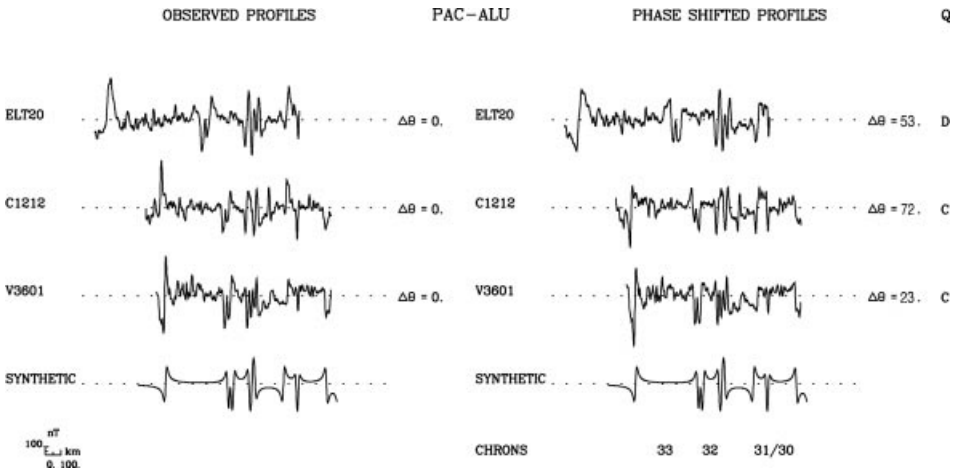

Figure 7. Profiles obtained over seafloor produced by Pacific–Aluk seafloor spreading. Original profiles are shown as recorded. The east longitude of the profiles decreases from the top to the bottom the figure. The synthetic profiles show the sequence from anomaly 33 to anomaly 30.

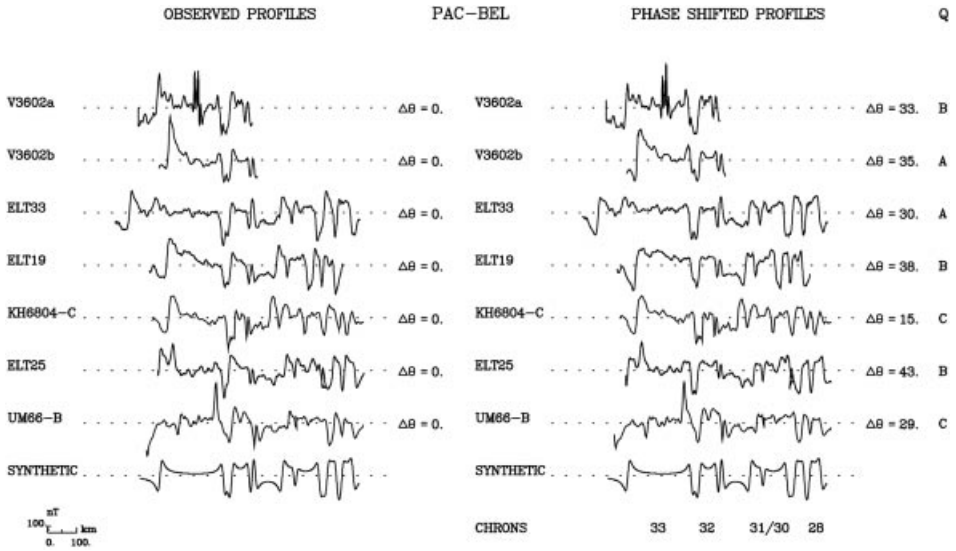

Figure 8. Profiles obtained over seafloor produced by Pacific–Bellingshausen seafloor spreading. The east longitude of the profiles decreases from the top to the bottom the figure.

are sufficient in number and well distributed over the Pacific plate, whereas the former method works well even if the data are sparse (Petronotis *et al.* 1992, 1994). The confidence limits are tested through the use of Monte Carlo simulations (Petronotis *et al.* 1992, 1994).

Because the data are of unequal quality due to varying amplitudes and noise that may be caused by rough seafloor topography, magnetic storms that occurred during the collection of the data, propagating rifts, the proximity of fracture zones, data gaps, etc., the first step is to assign each datum to a quality group of A, B, C, or D, with A being the best and D being the worst. A few additional possible crossings of anomaly 32 were rejected because the identification of the anomaly was suspect. Profiles with higher amplitudes and consistent appearances are generally included in groups A and B, whereas low-amplitude profiles such as those near the equator, profiles with atypical appearances or data gaps, and profiles digitized from published figures are included in groups C and D. The next step is to estimate the standard deviation of each of these groups separately by finding a best-fitting pole, anomalous skewness, and summed squared error for each group. The uncertainty then assigned to each datum is the standard deviation found for its group. The final pole is computed by combining the data from all the groups.

PROFILE DESCRIPTION AND SKEWNESS ESTIMATES

We present results from 108 crossings of anomaly 32: 19 recording Pacific–Kula spreading (Figs 2 and 3), 55 recording Pacific–Farallon spreading (Figs 2, 4, 5 and 6), three recording Pacific–Aluk spreading (Figs 2 and 7), 11 recording Pacific–Bellingshausen spreading (Figs 2 and 8), and 20 recording Pacific–Antarctic spreading (Figs 2 and 9).

Pacific–Kula crossings

We analysed 19 crossings of anomaly 32 on profiles over Pacific–Kula seafloor. One crossing is located west of the

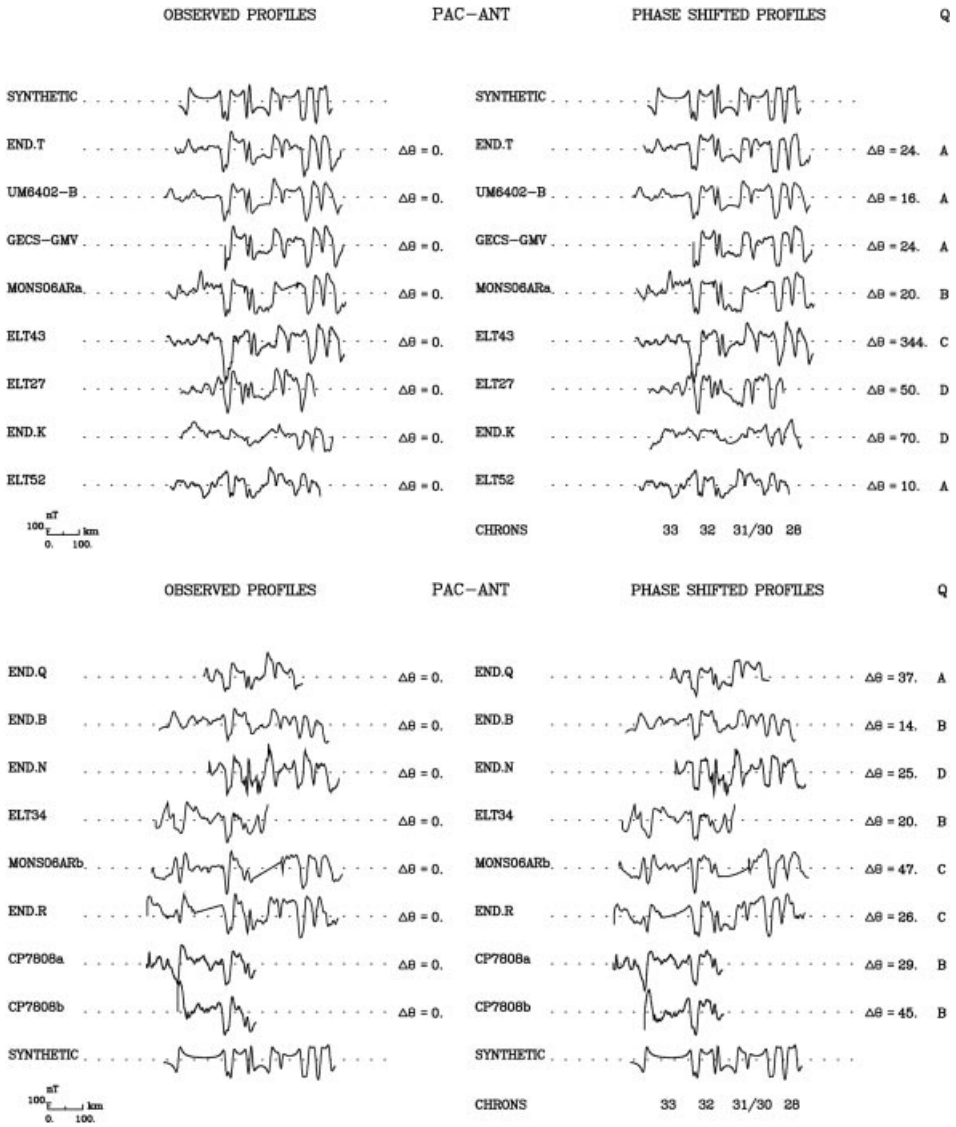

Figure 9. Profiles obtained over seafloor produced by Pacific–Antarctic seafloor spreading. The east longitude of the profiles decreases from the top to the bottom the figure.

Stalemate fracture zone, one between the Stalemate and Rat fracture zones, three between the Rat and Adak fracture zones, five between the Adak and Amlia fracture zones, and nine east of the Amlia fracture zone ('KU' in Fig. 2). The existence of the Adak fracture zone was first suggested by Grim & Erickson (1969) and later supported by Rea & Dixon (1983). Lonsdale (1988) presented a revised seafloor interpretation for the region south of the Aleutian trench that calls for fracture zones that are oblique to the anomaly pattern. His new interpretation applies only to anomaly 32A and younger anomalies, however, and still shows a north–south fracture zone adjacent to anomaly 32. In Fig. 2 we show the north–south version of the Adak fracture zone as in the map of Atwater & Severinghaus (1989).

The Pacific–Kula anomalies have high amplitudes (500–700 nT peak to trough) throughout the region. Thus, the estimation of the skewness of each of these anomaly crossings is straightforward, with most estimates of $\Delta\theta$ ranging from 86° to 112°, one estimate of 69°, and one estimate of 128° (Fig. 3). The nine category C profiles include profile SI932005a, in which there is no separation between anomaly 32A and the young end of anomaly 32; profile L878NP, in which the young end of anomaly 32 has an irregular appearance probably caused by the presence of a seamount observed in the bathymetry; and profiles GECS-BMV and CMAPPI5A, in which the anomaly 32 crossings are wider than expected. The unusual width of GECS-BMV and CMAPPI5A may be related to their proximity to the Adak fracture zone (Fig. 2).

Pacific–Farallon crossings

It is convenient to divide the profiles collected over seafloor produced by Pacific-Farallon spreading into three groups: northern (north of 22°N; 'NF' in Fig. 2); central (between the equator and 22°N; 'CF' in Fig. 2); and southern (south of 5°S; 'SF' in Fig. 2).

Northern Pacific–Farallon crossings

Of the 36 profiles analysed in this group, six lie south of the Great Magnetic Bight but north of the Surveyor fracture zone, one between the Surveyor and Mendocino fracture zones, one between the Pau and Pioneer fracture zones, 14 between the Pioneer and Murray fracture zones, and 14 between the Murray and Molokai fracture zones ('NF' in Fig. 2). These profiles typically have peak-to-trough amplitudes that range from 300–400 nT in the north to 100–200 nT in the south (Fig. 4). The phase shifts we estimate range from 15° to 111° with a gradual progression towards higher phase shifts from north to south (Fig. 4).

Profiles with atypical appearances north of the Pioneer fracture zone include C1109b, YAQ701, and KH7002b, which were given a C rating, and POL7004, which was given a D rating. Bathymetric data indicate the presence of seamounts or ridges, which probably affect the shape of C1109b, YAQ701, and POL7004. Between the Pioneer and Murray fracture zones, Atwater & Severinghaus (1989, especially their plate 3b) mapped a 'wandering small offset' and interpreted it as the long-term manifestation of persistent overlapping spreading centres (Macdonald *et al.* 1988). This extra anomaly contributes to the atypical appearance of profiles POL7103d, NOVA01AR, POL7103e, POL7103f, POL7103h, and POL7103j, which were assigned to quality category D, and can be further traced to the east of anomaly 32A on profiles POL7103g and POL7103i. Between the Murray and Molokai fracture zones, ELT30 and JPYN01BD were the only profiles whose low amplitude and atypical appearance warranted a D rating.

Central Pacific–Farallon crossings

The 15 profiles in this group lie south of the Molokai fracture zone and north of the Clipperton fracture zone ('CF' in Fig. 2). The peak-to-trough amplitudes range from 75 to 100 nT. As discussed by Acton & Gordon (1991) and Petronotis *et al.*

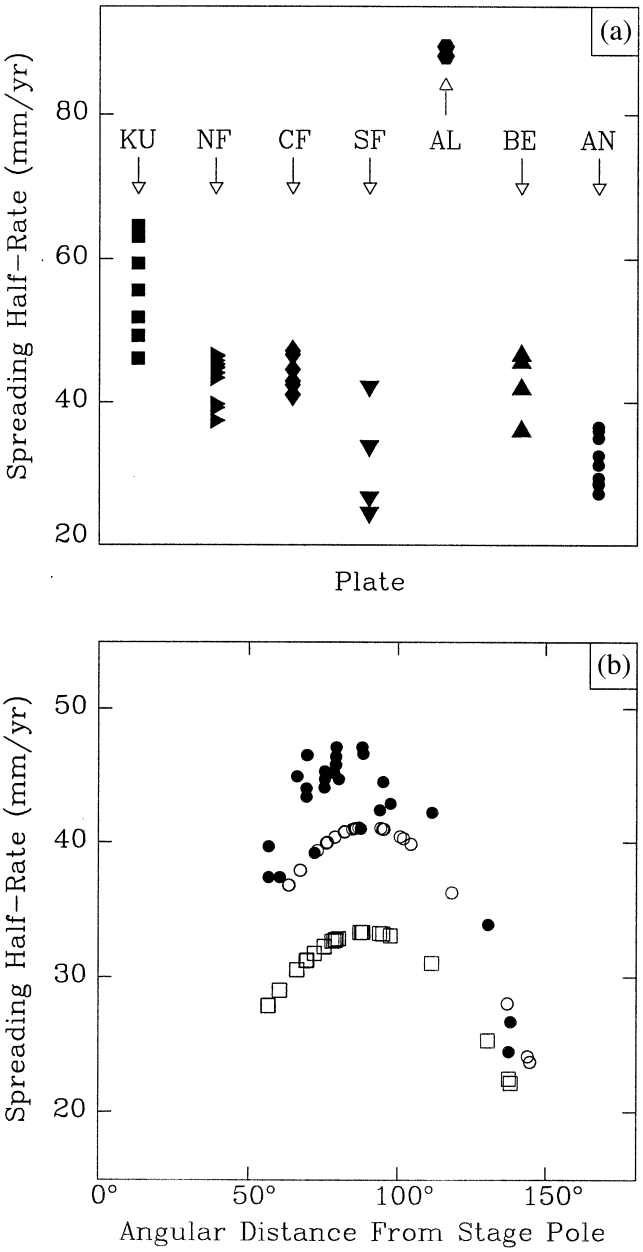

Figure 10. (a) Range of spreading half-rates estimated from the distance between the young end of anomaly 33 and the boundary between anomalies 30/31. The two-letter codes denote the seven geographical subgroups of data used in the text. (b) Observed (solid circles) and predicted [open circles: Engebretson *et al.* (1984); open squares: Rosa & Molnar (1988)] spreading half-rates versus distance from the stage pole of rotation for Pacific–Farallon profiles.

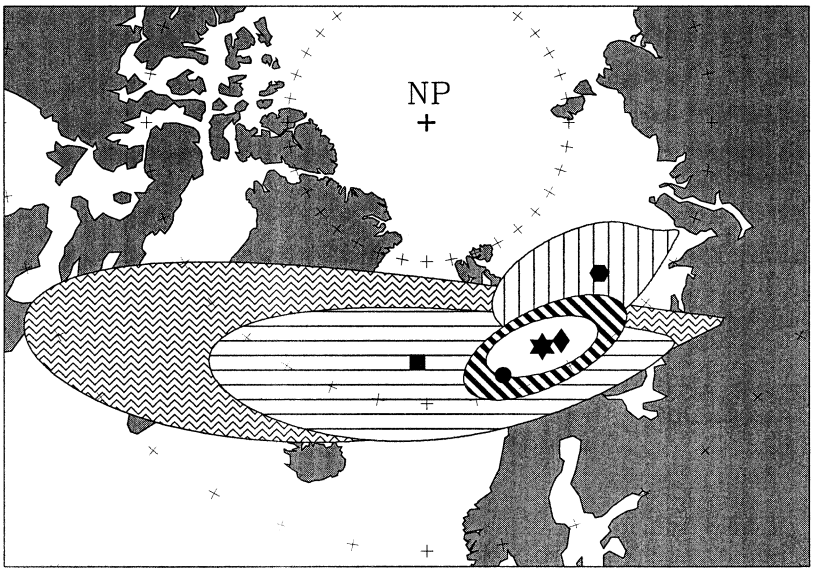

Figure 11. Palaeomagnetic poles and associated confidence limits for quality subgroups A (circle, horizontal stripes), B (square, zig-zag lines), C (diamond, diagonal stripes), and D (hexagon, vertical lines). The best-fitting pole from all data (star) and its associated 95 per cent confidence region (unshaded) are also shown. The confidence limits of subsets A–D were computed using the technique of constant-chi-square boundaries.

(1992), the identification of the anomaly sequence is made difficult by the low amplitudes, highly skewed shapes, and steep north–south gradient in skewness. By phase shifting these profiles, we are able to identify the anomaly sequence despite the low amplitudes.

Nine profiles are distributed along $\sim 6^\circ$ of latitude between the Molokai and Clarion fracture zones (Fig. 2) and provide the most important data because they bracket the palaeoequator ($\sim 18^\circ$N), where the effective inclinations change the fastest with latitude (Figs 10 and 11). Consequently they give tight constraints on the location of the palaeomagnetic pole. The six profiles between the Clarion and Clipperton fracture zones are slightly less important and provide useful information on the location of anomalies 28 to 33 in this region. Despite their low amplitudes, the deskewed crossings of anomaly 32 have a consistent appearance (Fig. 5). The phase shifts range from 90° to 160° in the northern group, and from 147° to 202° in the southern group. Uncertainties for these profiles were assigned conservatively: nine to category C and six to category D.

Southern Pacific–Farallon crossings

This group includes one profile between the Galapagos and Marquesas fracture zones and three profiles south of Austral fracture zone ('SF' in Fig. 2). The sparsity of crossings of anomaly 32 between the Galapagos and Austral fracture zones is mainly due to the presence of the Marquesas and Society island chains, which lie partly on chron 32 seafloor. These profiles have peak-to-trough amplitudes that increase from ~ 100 to ~ 200 nT from north to south (Fig. 6). Although the amplitudes are higher than for the central Pacific–Farallon group of profiles, the slow spreading rates make skewness analysis of this group just as challenging as for the central Farallon group. The phase shifts range from -49° to $+16^\circ$. One profile was rated category C, and three as category D. Profile ELT29 was assigned a D rating because its crossing of anomaly 32 is interrupted by a small data gap. The D rating of profiles POL6702 and C0905 was assigned for the atypical appearance of anomalies 31r, 32r and 32a.

Pacific–Aluk crossings

The three profiles in this group ('AL' in Fig. 2) lie just to the NE of the Heezen fracture zone, have moderate amplitudes of 350–400 nT, and phase shifts of 23°, 53° and 72°. Two of the profiles were given a C rating because they have atypical appearances, which are caused by rough seafloor on the young side of anomaly 32. Profile ELT20 was given a D rating because it crosses anomaly 32 twice. Of the two crossings on this profile only the eastern one appears complete and was the only one phase-shifted (Fig. 7). An added complication in this region is the uncertainty associated with the azimuth of the anomaly 32 lineation. The seafloor formed by Pacific–Aluk spreading covers a small region, which is traversed by few profiles. The azimuth used in our calculations was estimated from Fig. 3 of Cande *et al.* (1982).

Pacific–Bellingshausen crossings

The 11 profiles in this group lie SW of the Heezen fracture zone and NE of the magnetic bight separating seafloor created by Pacific–Antarctic spreading from seafloor created by Pacific–Bellingshausen spreading (at 185°E, between the Endeavor and Udintsev fracture zones; 'BE' in Fig. 2) (Stock & Molnar 1987). These profiles are of high quality because of their high amplitudes, which increase from ~ 400 to ~ 500 nT from east to west (Fig. 8). Profile KH6804-C, which has a narrower than expected crossing of anomaly 32 presumably caused by a change in the ship-track direction, was given a C rating. The category D profiles consist of those digitized from published figures (Christoffel & Falconer 1972). The phase shifts range from 7° to 48° (Fig. 8).

Pacific–Antarctic crossings

The 20 profiles of this group extend from NE of the Endeavor fracture zone to SW of fracture zone XIII ('AN' in Fig. 2) and have amplitudes that decrease from ~500 to ~250 nT from NE to SW (Fig. 9). The anomaly crossings are of moderate to high quality, with five rated category A, five category B, three category C, and seven category D. Profiles ELT27 and END.N were rated D because of the atypical appearance of the young end of anomaly 32. Profile END.K was penalized for its relatively low amplitude, and ELT43 for the atypical appearance of the older end of anomaly 32. Four of the category D profiles were digitized from published figures (Christoffel & Falconer 1972). The phase shifts range from -16° to 85°, with most between 20° and 50° (Fig. 9).

Spreading rates

As a test of the consistency of our interpretation of the magnetic anomalies and to provide a basis for analysing the dependence of anomalous skewness on spreading rate, we examined the variation in spreading rates along the ancient Pacific–Kula, Pacific–Farallon, Pacific–Aluk, Pacific–Bellingshausen, and Pacific–Antarctic spreading centres. Half-rates were estimated by comparing the observed anomaly 30/31 to 33 sequence with synthetic magnetic-anomaly profiles.

Estimated Pacific–Kula half-rates range from 46 to 65 mm yr^{-1} (Fig. 10), which are similar to, or slightly faster than, the 47–53 mm yr^{-1} implied by the anomaly 33–30 stage pole and angular rate of Engebretson *et al.* (1984) and about double the 27–34 mm yr^{-1} rate implied by the anomaly

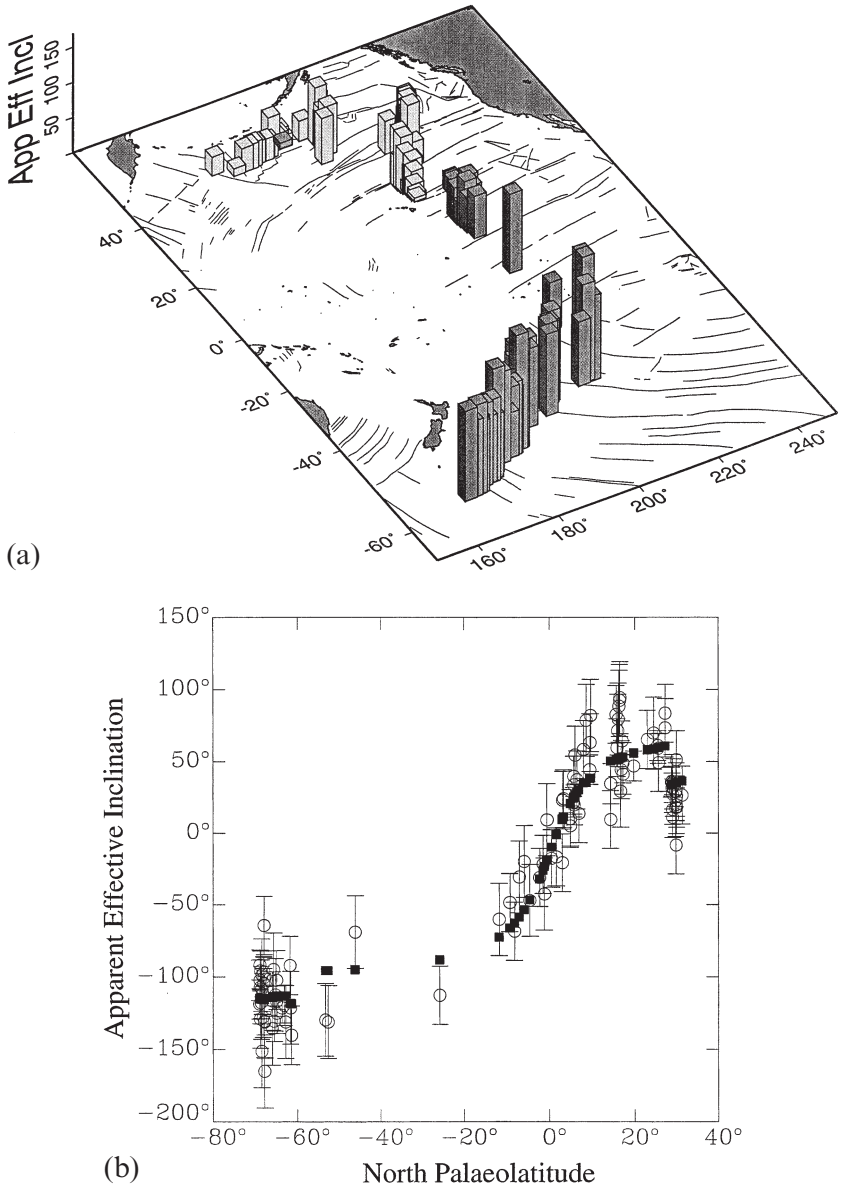

Figure 12. (a) Apparent effective remanent inclinations shown in their present geographical locations. The light bars correspond to values between 5° and 94° and the dark bars to values between -8 and -165°. (b) Observed (open circles) and modelled (solid squares) apparent effective remanent inclinations versus palaeolatitude. The modelled apparent effective remanent inclinations are calculated from the single best-fitting pole and anomalous skewness determined from the entire data set. The excellent data coverage around the palaeoequator where the effective inclinations change the fastest results in tight confidence limits for the palaeomagnetic pole.

32–30/31 stage pole and angle of Rosa & Molnar (1988). Estimated half-rates for northern Pacific–Farallon spreading range from 37 to 47 mm y^{-1}, those for central Pacific–Farallon spreading range from 41 to 47 mm yr^{-1}, and those for southern Pacific–Farallon spreading range from 42 mm yr^{-1} at 8°S to 26 mm yr^{-1} at 35°S (Fig. 10). The northern and central half-rates are slightly faster than those calculated from the anomaly 34–25 stage pole and angular rate of Engebretson *et al.* (1984), and ~35 per cent faster than those calculated from the anomaly 30/31–25 stage pole and angle of Rosa & Molnar (1988) (Fig. 10). The southernmost Pacific–Farallon half-rates are similar to the half-rates calculated from both models (Fig. 10). The half-rates estimated for Pacific–Aluk spreading are 89 mm yr^{-1}, those for Pacific–Bellingshausen spreading range from 42 to 47 mm yr^{-1}, and those for Pacific–Antarctic spreading range from 36 mm yr^{-1} east of the Endeavor fracture zone to 29 mm yr^{-1} west of fracture zone XIII (Fig. 10).

RESULTS

Main palaeomagnetic results

The standard deviations estimated by separately inverting each group of effective inclinations are 10.4° for the 18 data in category A, 14.0° for the 19 data in category B, 20.2° for the 41 data in category C, and 25.1° for the 30 data in category D. The best-fitting poles from only the data in each group differ insignificantly from one another (Fig. 11). The combined best-fitting pole, found from all 108 data with each datum assigned an uncertainty equal to the standard deviation of its group, is located at 71.2°N, 26.8°E and has a 95 per cent confidence ellipse with a 4.0° major semi-axis striking N98°E and a 1.8° minor semi-axis (Fig. 11). The best-fitting value of anomalous skewness is 14.2° ± 3.7° (95 per cent confidence level) (Table 1).

Allowing anomalous skewness to adjust instead of fixing it at zero decreases χ^2 from 165.2 to 108.7, which is a 34 per cent reduction of variance and gives a value of the F statistic of 56.5 with 1 versus 105 degrees of freedom. The probability of F being this large or larger by chance is 2×10^{-11}. This by no means proves that anomalous skewness is uniform and independent of spreading rate or other variables, but it does show that this simple one-parameter adjustment gives a highly significant improvement in fit and can explain a considerable fraction of the variance in the data.

Each apparent effective inclination is compared with its corresponding model effective inclination in Fig. 12, where both are plotted against site palaeolatitude calculated from the best-fitting palaeomagnetic pole. Model effective inclinations range from −116° for the easternmost Pacific–Antarctic crossings to +61° for the northernmost Pacific–Farallon crossings. The data from profiles between the Molokai and Clarion fracture zones, with 33.6 per cent of the total importance, contribute more information than do those from any other region of similar size (Fig. 13, Table 1). The good data coverage near the palaeoequator, where effective inclination changes the fastest with palaeolatitude, accounts for the small confidence region of the palaeomagnetic pole. At low palaeolatitudes, small changes in estimated pole position cause large changes in predicted value of effective inclination (Acton & Gordon 1991). This effect outweighs the larger uncertainties that we assign to these low-palaeolatitude data. The new palaeomagnetic pole implies that the palaeoequator lies about midway between the Molokai and Clarion fracture zones.

The second largest information contribution, 21 per cent, comes from the corridor between the Murray and Molokai fracture zones. The Pacific–Antarctic data contribute 14.7 per cent, the Pacific–Kula data 8.2 per cent, the Pacific–Bellingshausen data 7.4 per cent, the southern Pacific–Farallon data 1.4 per cent, and the Pacific–Aluk data 1.0 per cent. The gap in southern Pacific–Farallon data falls where the effective inclination curve becomes almost level (Fig. 12b); filling this gap would contribute little new information to the pole position.

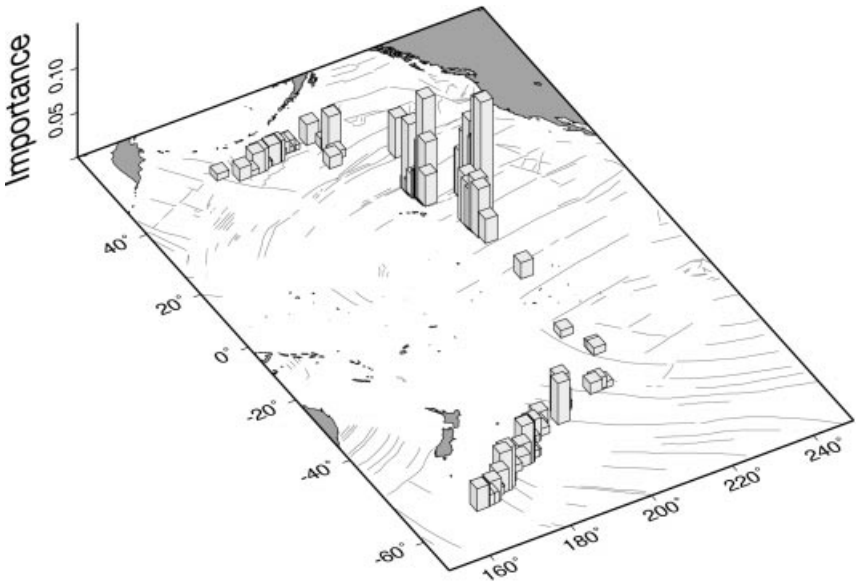

Figure 13. Data importances shown in their present geographical locations. The high values between ~3°S and 10°N show the high information content of the low-palaeolatitude data.

Regional constraints on the pole position and anomalous skewness are illustrated in Fig. 14. To make these figures, the data were first divided into the seven tectonic regions (Kula, north Farallon, central Farallon, south Farallon, Aluk, Bellingshausen, and Antarctic) discussed above. The two highest-information regions, north Farallon and central Farallon, were further divided into three and two parts, respectively. 10 great semicircles, each of which is the locus of pole positions consistent with the mean effective inclination of a region, are shown in Fig. 14(a) with no adjustment for anomalous skewness. If there were no uncertainty in the data and if there were no anomalous skewness, the great semicircles would intersect at a point, which they do not. Fig. 14(b) shows the same 10 great semicircles after adjustment for the best estimate of anomalous skewness. Although they still do not intersect at a point, their dispersion about the best-fitting pole is greatly reduced.

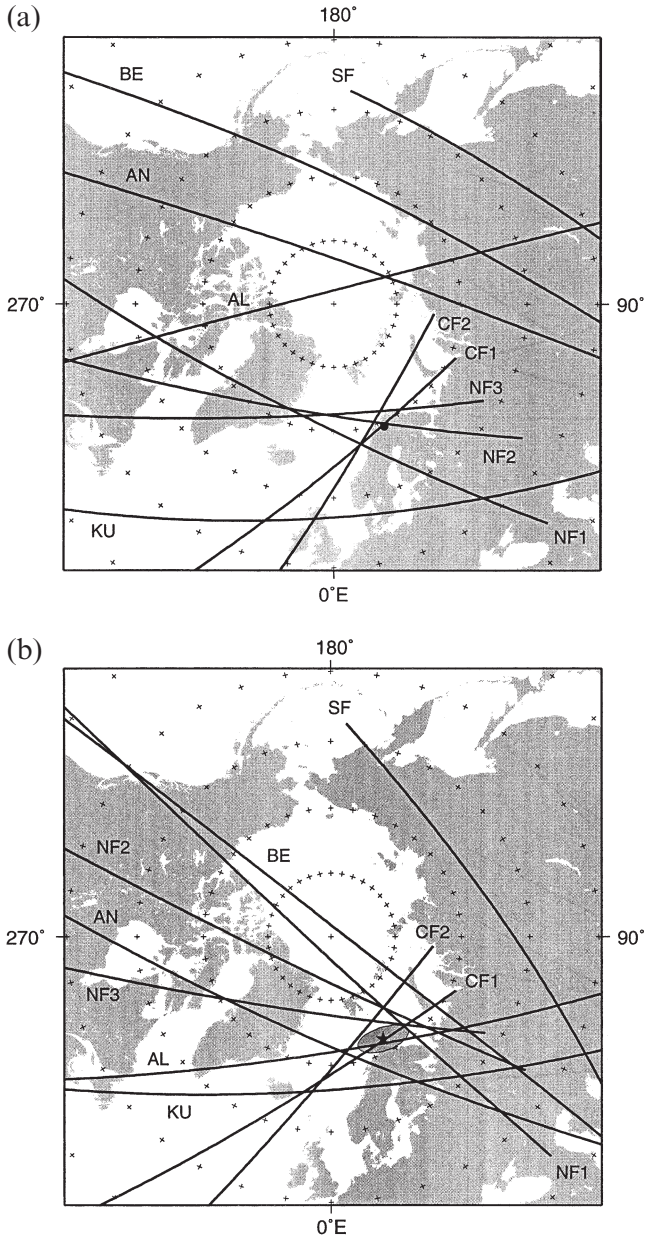

Figure 14. (a) Map of the northern polar region showing loci of pole positions consistent with the mean effective inclination of each of the seven geographical subregions. Profile KU is representative of the Pacific–Kula region; profiles NF1, NF2, NF3, CF1, CF2, and SF of the northern, central, and southern Pacific–Farallon regions, respectively; profile AL of the Pacific–Aluk region; profile BE of the Pacific–Bellingshausen region; and profile AN of the Pacific–Antarctic region. For anomalous skewness equal to zero the best-fitting pole is located at 69.3°N, 22.5°E. (b) For anomalous skewness equal to its best-fitting value (14.2°), the agreement of the great semicircles improves, with only the southern Pacific–Farallon great semicircle still showing a discrepancy. Tick marks are shown every 10° (stereographic projection).

A possible source of systematic error in this type of analysis is the magnetic lineation azimuth used. To investigate the sensitivity of the results to the lineation azimuth we recalculated the pole and anomalous skewness using different azimuths at each site. We inverted 10 additional synthetic data sets in which the lineation azimuths vary from $-6°$ to $+6°$ relative to the values calculated from published plate-motion models. The results of this experiment are shown in Fig. 15. The synthetic values of anomalous skewness are 0.5° to 1.6° different from the preferred value, well within the assigned 95 per cent confidence limits. Because large consistent errors in the estimate of lineation azimuth seem unlikely given the consistency of all the plate-motion models that are available, it seems unlikely that a consistent error in lineation azimuth could bias the pole by more than the degree or so of variation shown in Fig. 15(a). It is more likely that there are small uncorrelated variations in lineation azimuth, which would produce even smaller changes in the location of the pole than are shown in Fig. 15(a). A systematic error in lineation azimuth would cause the uncertainties in the chron 32 pole to be slightly overestimated or underestimated if the true azimuths are respectively clockwise or counterclockwise of our estimates.

As expected from the large number of data and their good geographical distribution, the confidence region of the pole obtained from the linear propagation of errors is an excellent approximation of the region obtained from the constant-chi-square boundaries technique (Fig. 16a). The results from Monte Carlo simulations further corroborate the confidence limits found from the linear propagation of errors. Of the 10 000 simulated best-fitting poles, 9457 fell within the 95 per cent confidence limits (Fig. 16b).

Anomalous skewness versus spreading rate

Prior studies indicate that anomalous skewness increases as spreading rate decreases (Cande 1976, 1978; Roest *et al.* 1992; Dyment *et al.* 1994). Here we use our data to examine further whether and how anomalous skewness varies with spreading rate. First, we obtain an empirical relationship between anomalous skewness and spreading rate from the data compiled by Roest *et al.* (1992), from the value of anomalous skewness obtained here, and from the average spreading rate of the profiles we analysed. We determined a best-fitting line from a data set comprising our mean result for anomaly 32 plus the data compiled by Roest *et al.* (1992) for the anomalous skewness of anomalies 33 and 34 versus spreading rate. That best-fitting line is given by the following equation (Fig. 17a):

$$\theta_a = 60.68° - 1.037u, \quad (4)$$

where u is the spreading half-rate in mm yr^{-1}. This estimate is dominated by the anomalous skewness of anomalies 33 and

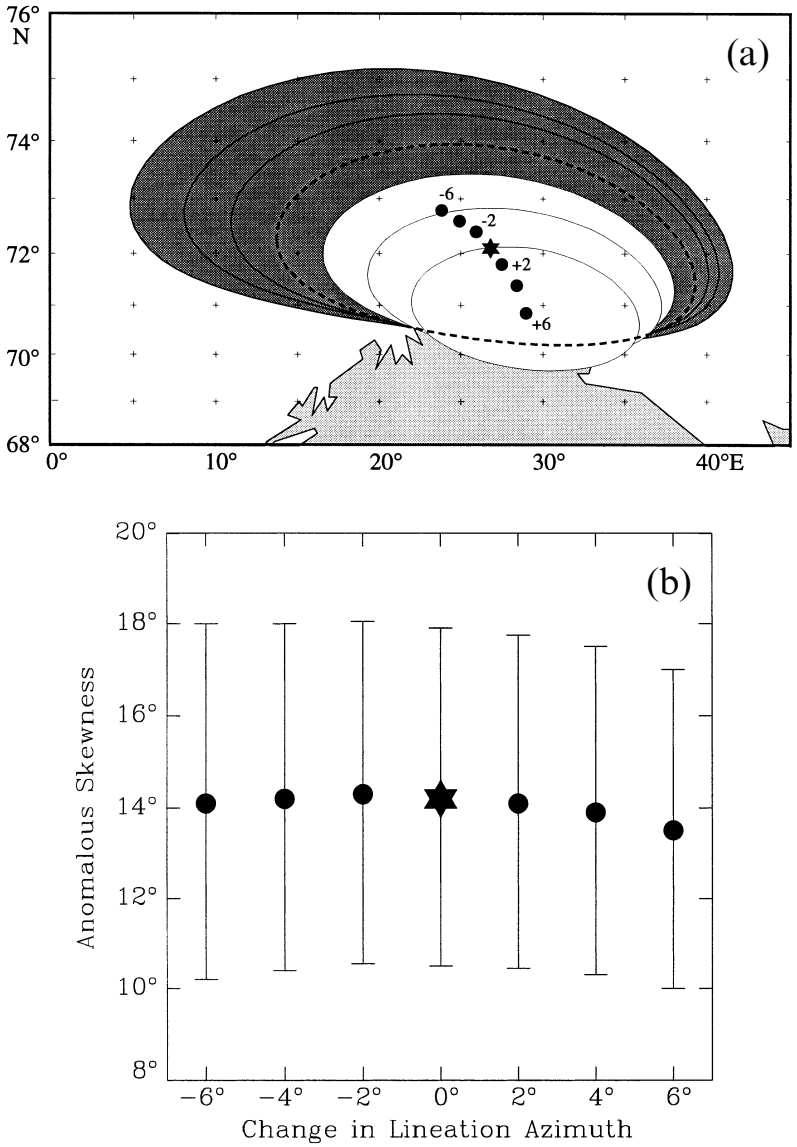

Figure 15. Inversions of synthetic data sets whose azimuths have been altered by $-6°$ to $+6°$ relative to the values calculated from published plate-motion models. (a) Geographical locations of palaeomagnetic poles. The shaded confidence regions correspond to $-6°$, $-4°$, and $-2°$ changes in azimuth. The unshaded confidence regions correspond to $+2°$, $+4°$, and $+6°$ changes in azimuth. The dashed outline represents the 95 per cent confidence region of the preferred pole. (b) Anomalous skewness values with 95 per cent confidence limits.

34 and may not apply to anomaly 32. We can use this equation to estimate a correction for anomalous skewness as a function of the spreading half-rate for an individual crossing of anomaly 32. When this correction is applied to the apparent effective inclinations for anomaly 32, the fit of the model to the data becomes much worse, with χ^2 increasing from 108.7 to 181.7. The corrected pole moves westwards to 71.5°N, 19.6°E, still within the 95 per cent confidence region of the preferred pole.

Second, we test whether there is a linear relationship between anomalous skewness and spreading rate in our data. Surprisingly, the best-fitting straight line ($\chi^2 = 102.4$) for anomalous skewness versus spreading rate has a positive slope (Fig. 17b) and is described by the following equation (Fig. 17a):

$$\theta_a = -2.42^\circ + 0.383u. \quad (5)$$

The slope term has 95 per cent confidence limits of ± 0.312 and differs significantly from zero. The corrected pole moves eastwards to 72.3°N, 28.9°E, still within the 95 per cent confidence region of the preferred pole.

We also tested for any trend in residual skewness (relative to our best-fitting model assuming no spreading rate dependence of anomalous skewness) versus spreading half-rate. We find only an insignificant correlation (Fig. 18). Because independent data, as well as published models of seafloor magnetization with non-vertical polarity boundaries, indicate that any slope should not be positive but negative, we prefer to use the pole obtained assuming that anomalous skewness is independent of spreading rate.

Published estimates of anomalous skewness as a function of spreading rate for anomalies 5 to 21 (Fig. 17) indicate only a weak dependence for half-rates exceeding ~ 20 mm yr^{-1}, but a strong dependence for half-rates less than ~ 20 mm yr^{-1} (Fig. 17). Perhaps the spreading rate dependence of anomalous skewness for anomaly 32 is more like that for anomalies 5 to 21

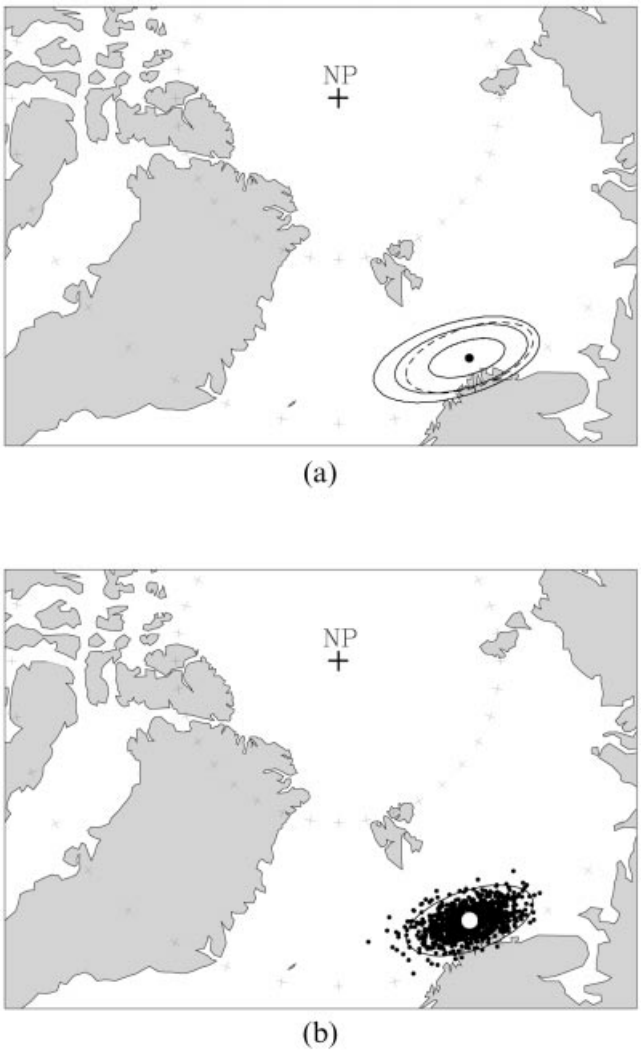

Figure 16. (a) Map of the northern polar region showing the chron 32 pole with its confidence regions. The dashed line is the 95 per cent confidence ellipse obtained from linear propagation of errors. The solid lines are the regions corresponding to the standard error (closest to the pole), 95 per cent, and 99 per cent (farthest from the pole) confidence levels, respectively, and were calculated using constant contours of χ^2 (Petronotis *et al.* 1992). The 95 per cent confidence regions calculated using the two different methods are in excellent agreement. (b) Monte Carlo simulations: 9457 out of 10 000 simulated poles were included within the 95 per cent confidence limits of the pole. Here, we show a representative subset of 1000 simulations.

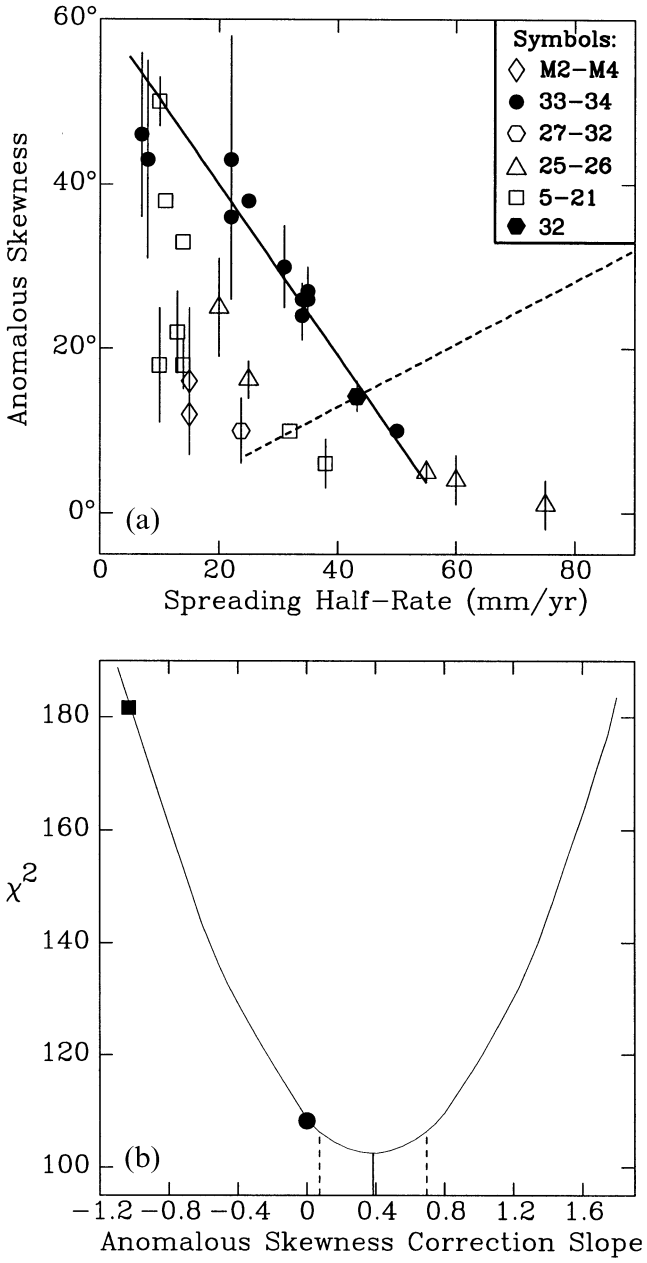

Figure 17. (a) Dependence of anomalous skewness on spreading rate as inferred from the results of many studies (modified from Roest *et al.* 1992; Petronotis *et al.* 1994). Slow spreading rates tend to have higher values of anomalous skewness for a given anomaly than do fast spreading rates. The chron 32 estimate from this paper is shown by the solid hexagon at the average half-rate of all our data. The solid line represents a least-squares straight-line fit (eq. 4) to the 32 and 33–34 data (solid symbols). The dashed line represents the linear correction that best fits the chron 32 effective inclinations only (eq. 5). (b) Experiment conducted to determine which linear correction best fits the chron 32 effective inclinations. We obtained the minimum χ^2 for a slope of $0.383^\circ \pm 0.312^\circ$ (95 per cent confidence level) of anomalous skewness per mm yr^{-1} of spreading half-rate. The square represents the χ^2 value obtained by applying the linear correction calculated from the least-squares line fit to the 32 and 33–34 data (solid line above). The circle represents the value obtained for no correction (i.e. for the preferred pole).

than like that for anomalies 33 and 34. If so, given that few of our data for anomaly 32 are from half-rates less than 20 mm yr^{-1}, any spreading rate dependence is likely to be weak. Moreover, the range of spreading rates sampled by our data is very narrow, with 97 of the 108 skewness estimates coming from profiles with half-rates between 28 and 47 mm yr^{-1}, and the spreading rate dependence, if any, may not be resolvable. It is interesting to note that the two crossings with the slowest rates have large negative residuals, consistent with the expected larger values of anomalous skewness (Fig. 18), but there are far too few crossings with slow rates to draw any firm conclusions.

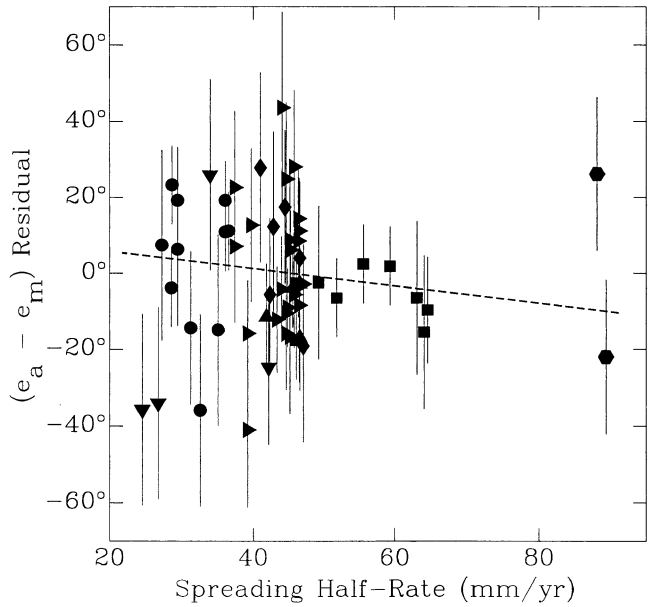

Figure 18. Effective inclination residuals versus spreading half-rates. The line that best fits the data has an intercept of 9.697 and a slope of -0.220 ± 0.365 (95 per cent confidence limits). The various subregions are represented by squares (Kula), right-pointing triangles (northern Farallon), diamonds (central Farallon), downward-pointing triangles (southern Farallon), hexagons (Aluk), upward-pointing triangles (Bellingshausen), and circles (Antarctica).

Comparison with other palaeomagnetic and palaeolatitude data

The new pole differs insignificantly from, but indicates a few degrees less northward motion of the Pacific plate than, other Maastrichtian-age palaeocolatitude and palaeoequatorial data (Fig. 19). The new pole differs significantly, however, from presumably coeval poles obtained from seamount magnetism. Fig. 19 shows the locations of poles for seven seamounts with ages between 65 and 80 Ma. Except for two poles determined for the Von Valtier seamount by Hildebrand & Parker (1987), the seamount poles are grouped in a swath lying west, southwest, and south of our new pole. All the seamount poles lie outside the 95 per cent confidence limit of our new pole. The four seamount poles having 95 per cent confidence regions differ significantly from our new pole. Moreover, many of the seamount poles are inconsistent with one another. Among the four distinct seamount poles having confidence regions, four of the six possible comparisons indicate significant differences. The only two insignificant differences are between Erimo and the two other poles included in its large confidence region.

Parker (1991) argues that palaeopoles determined from seamount surveys are probably much less reliable than has been assumed in prior work, including his own work based on the semi-norm minimization approach. He cites results from dredging that indicate that seamounts (as well as the seafloor) contain many pockets of highly magnetic material, which implies that a uniform model of magnetization, as has been assumed in estimating nearly all seamount poles, is a poor

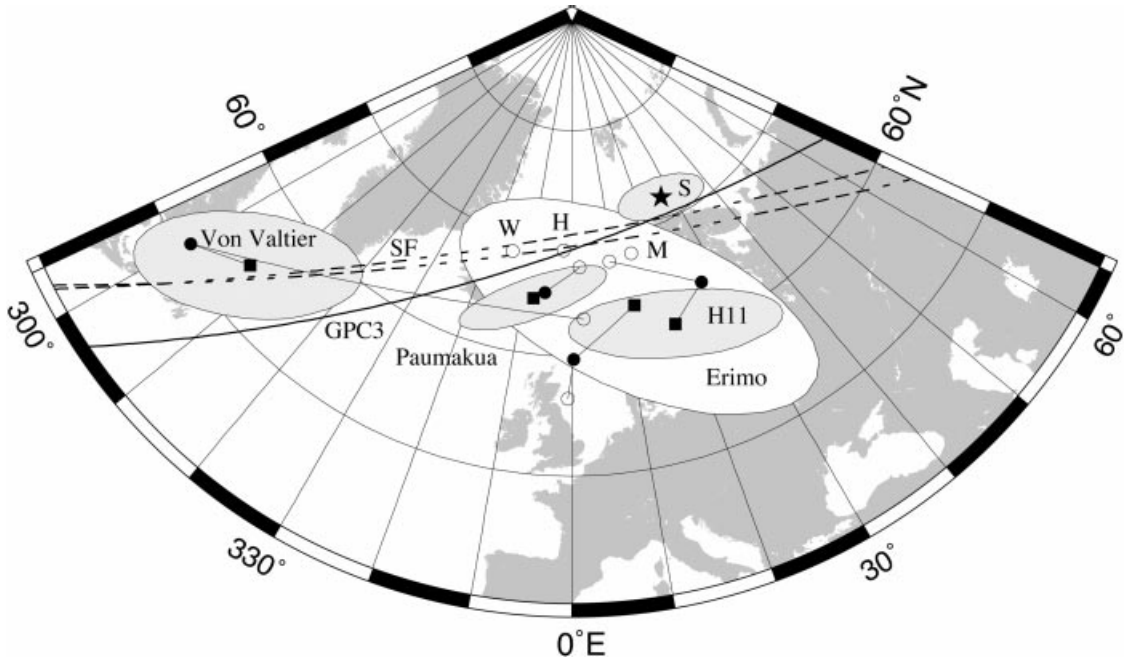

Figure 19. Comparison of Maastrichtian palaeomagnetic data. The star (S) represents the chron 32 skewness pole. The solid and dashed lines represent the palaeolatitudes inferred from Giant Piston Core 3 and palaeoequatorial sediment facies data from DSDP sites 171 and 313, respectively. Seamount poles are shown for Paumakua, Wageman (W), H11, Haydn (H), Mendelssohn (M), Erimo, and Von Valtier seamounts. Multiple symbols are used to represent seamount poles calculated for the same seamount from different data sets or by different methods: least-squares (open circles, Sager & Pringle 1988), least-squares (solid circles, Hildebrand & Parker 1987), and semi-norm minimization (solid squares, Hildebrand & Parker 1987). Seamount pole 95 per cent confidence regions are shown for those poles calculated by semi-norm minimization. Meridians and parallels are shown every 10°.

Table 1. Chron 32 Pole (72.1–73.3 Ma).

Pole Location: 72.1° N, 26.8° E, Anomalous Skewness = 14.2° ± 3.7°

95% Confidence Ellipse		
Semi Axis	Length of Semiaxis	Orientation (cw from N)
Major	4.0°	98.0°
Minor	1.8°	8.0°

χ^2 = 108.67 with 105 degrees of freedom

Profile	Lat (°N)	Long (°E)	$\Delta\theta$ (°)	Azim (°)	e_a (°)	σ_θ (°)	e_m (°)	Residual(°)	Importance
Seafloor Created by Pacific-Kula Spreading									
West of Stalemate F.Z.									
c1108	46.9	173.4	95.0	82.0	26.5	20.2	36.4	-9.9	0.007
East of Stalemate F.Z. and West of Rat F.Z.									
c1008	45.1	177.5	112.0	86.0	10.9	14.0	33.9	-23.0	0.014
East of Rat F.Z. and West of Amlia F.Z.									
si932005.a	45.2	179.5	88.0	88.0	34.6	20.2	33.9	0.8	0.006
v2006	45.2	180.8	87.0	89.0	35.6	10.4	33.7	1.9	0.024
pol6971	45.4	181.9	86.0	89.0	36.2	10.4	33.8	2.5	0.024
gecs-bmv	45.8	183.0	90.0	90.0	31.8	20.2	34.2	-2.4	0.006
cmappi5a	45.8	183.2	90.0	90.0	31.8	20.2	34.2	-2.4	0.006
c1109.a	45.8	185.3	90.0	92.0	31.5	10.4	34.0	-2.5	0.023
pol6829.c	45.9	185.5	105.0	92.0	16.5	10.4	34.0	-17.6	0.023
pol6829.d	46.0	186.5	94.0	93.0	27.3	10.4	34.1	-6.8	0.023
East of Amlia F.Z. and West of the Great Magnetic Bight									
cmapsu5a	47.1	187.8	69.0	94.0	51.2	20.2	35.4	15.8	0.006
c1220	47.2	188.7	102.0	94.0	18.0	14.0	35.4	-17.4	0.013
c1010	47.2	189.6	100.0	94.0	19.9	20.2	35.2	-15.4	0.006
pol6829.a	47.2	190.0	97.0	95.0	22.8	14.0	35.3	-12.5	0.013
kh7002.a	47.3	190.0	94.0	95.0	25.8	14.0	35.4	-9.6	0.013
l878np	47.2	190.1	91.0	96.0	28.9	20.2	35.3	-6.4	0.006
pol6829.b	47.2	191.0	128.0	96.0	-8.3	20.2	35.3	-43.6	0.006
pol7103.m	47.1	191.1	102.0	96.0	17.8	20.2	35.2	-17.4	0.006
v2112	47.3	195.9	90.0	99.0	28.8	10.4	35.3	-6.5	0.023
Subtotal									0.248
Seafloor Created by Pacific-Farallon Spreading (Northern)									
South of the Great Magnetic Bight and North of Surveyor F.Z.									
c1109.b	45.0	198.0	25.0	161.0	83.5	20.2	60.9	22.6	0.011
yaq701	45.0	198.2	35.0	161.0	73.4	20.2	60.8	12.6	0.011
kh7002.b	43.4	198.0	60.0	161.0	49.1	20.2	59.8	-10.7	0.012
si932005.b	43.3	198.1	50.0	161.0	59.1	10.4	59.7	-0.6	0.045
pptu11wt	43.2	198.0	48.0	161.0	60.9	10.4	59.6	1.3	0.045
pol7004	42.2	198.4	40.0	161.0	69.7	25.1	58.7	10.9	0.008
South of Surveyor F.Z. and North of Mendocino F.Z.									
pol7103.a	40.6	196.3	45.0	161.0	65.3	20.2	58.3	7.1	0.013
South of Pau F.Z. and North of Pioneer F.Z.									
pol7201	37.6	210.2	62.0	166.0	46.8	10.4	55.8	-9.1	0.044
South of Pioneer F.Z. and North of Murray F.Z.									
lusi01ar	35.0	212.6	68.0	167.0	41.1	14.0	53.3	-12.2	0.025
indp01wt	35.0	212.7	60.0	167.0	49.0	14.0	53.2	-4.2	0.025
pol7103.b	34.8	212.7	45.0	167.0	64.1	14.0	52.9	11.2	0.025
pol7103.c	34.6	212.7	65.0	167.0	44.2	20.2	52.7	-8.5	0.012
pol7103.d	34.4	212.8	80.0	167.0	29.2	25.1	52.5	-23.2	0.008
nova01ar	34.3	212.6	15.0	167.0	94.3	25.1	52.3	42.0	0.008
pol7103.e	34.2	212.6	17.0	167.0	92.3	25.1	52.3	40.0	0.008
pol7103.f	34.1	212.7	21.0	167.0	88.4	25.1	52.0	36.3	0.008
pol7103.h	33.9	212.7	30.0	167.0	79.4	25.1	51.8	27.6	0.008
pol7103.j	33.8	212.8	38.0	167.0	71.5	25.1	51.5	19.9	0.008
pol7103.g	33.6	212.8	50.0	167.0	59.6	20.2	51.3	8.3	0.012
pol7103.i	33.4	212.9	27.0	167.0	82.6	20.2	51.0	31.6	0.012
pol7103.k	32.1	213.0	100.0	168.0	9.5	20.2	50.5	-41.0	0.014
gecs-amv	32.1	213.1	75.0	168.0	34.5	14.0	50.3	-15.8	0.028
South of Murray F.Z. and North of Molokai F.Z.									
elt30	27.5	206.4	32.0	165.0	82.0	25.1	38.5	43.6	0.013
pol7103.l	27.4	206.6	51.0	165.0	63.1	20.2	38.2	24.8	0.021
c1301.a	27.3	206.5	70.0	165.0	44.2	10.4	38.0	6.2	0.079
jpyn01bd	26.5	206.6	36.0	165.0	78.6	25.1	35.4	43.3	0.014
v2004	25.9	206.8	56.0	166.0	58.2	20.2	35.1	23.1	0.025
rndb01wt	24.8	207.3	101.0	166.0	13.6	20.2	30.3	-16.7	0.027
si933010	24.3	207.3	78.0	166.0	37.2	20.2	28.4	8.8	0.029
erdc01wt	23.9	207.4	61.0	166.0	54.4	20.2	26.4	28.0	0.030
c1301.b	23.7	207.4	96.0	166.0	19.6	14.0	25.2	-5.6	0.064
dsdp18gc	23.6	207.5	76.0	166.0	39.6	14.0	25.2	14.4	0.064
um6503-a	23.6	207.5	82.0	166.0	33.6	20.2	25.1	8.5	0.031
78070800	23.5	207.6	94.0	166.0	21.6	10.4	24.4	-2.8	0.118
dsdp55gc	22.8	207.7	111.0	166.0	5.0	14.0	20.8	-15.8	0.071
scan05ar	22.8	207.7	106.0	166.0	10.2	20.2	20.6	-10.4	0.034
Subtotal									1.010
Seafloor Created by Pacific-Farallon Spreading (Central)									
South of Molokai F.Z. and North of Clarion F.Z.									
c2002	21.0	215.5	90.0	169.0	24.1	20.2	11.7	12.5	0.049
78123001	20.8	215.6	91.0	169.0	23.1	20.2	10.2	12.9	0.051
76101000	20.7	215.6	135.0	169.0	-20.7	20.2	9.8	-30.5	0.052

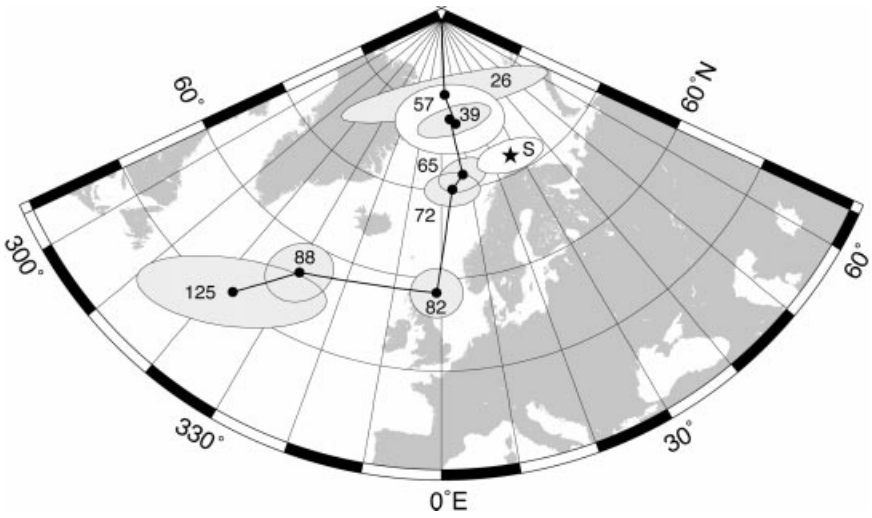

Figure 20. Apparent polar wander path of the Pacific plate. The poles shown are a 125 Ma pole (Petronotis *et al.* 1992), 72 Ma, 82 Ma, and 88 Ma poles (Sager & Pringle 1988), the 73 Ma skewness pole calculated here, a 65 Ma pole (Acton & Gordon 1991), a 57 Ma skewness pole (Petronotis *et al.* 1994), a 39 Ma pole (Acton & Gordon 1994), and a 26 Ma pole (Acton & Gordon 1994) calculated from palaeolatitude data. The chron 32 pole suggests very rapid northward APW ($1.89° \pm 0.38°$ Myr^{-1}) from 82 to 73 Ma and complex APW between 73 and 57 Ma. Meridians and parallels are shown every 10°.

Table 1. (*Continued.*)

71042612	19.3	215.7	132.0	169.0	-16.6	20.2	-0.9	-15.7	0.076
elt31	18.2	215.8	134.0	169.0	-17.7	20.2	-9.7	-8.0	0.096
um6503-b	17.1	216.6	108.0	169.0	9.3	25.1	-18.5	27.8	0.073
epll01wt	16.5	216.7	160.0	169.0	-42.4	25.1	-23.2	-19.2	0.077
dpsn01wt	16.2	216.8	140.0	169.0	-21.8	20.2	-25.8	4.1	0.121
72081900	15.4	217.0	150.0	169.0	-31.0	20.2	-31.9	0.9	0.123
South of Clarion F.Z. and North of Clipperton F.Z.									
v2113	13.3	211.9	172.0	167.0	-47.0	25.1	-46.6	-0.4	0.056
swan-1ar	12.0	211.9	147.0	167.0	-19.8	25.1	-53.3	33.5	0.050
scan02ar	10.8	212.1	160.0	167.0	-30.6	25.1	-58.4	27.8	0.044
87001611	9.7	212.3	200.0	167.0	-68.3	20.2	-62.7	-5.7	0.060
nova06ho	8.6	212.3	183.0	167.0	-48.5	20.2	-66.0	17.5	0.054
dsdp08gc	6.1	212.7	202.0	167.0	-60.2	25.1	-72.4	12.2	0.027
Subtotal									1.009
Seafloor Created by Pacific-Farallon Spreading (Southern)									
South of Galapagos F.Z. and North of Marquesas F.Z.									
pptu03wt	-8.0	213.4	320.0	166.0	-112.8	20.2	-88.0	-24.7	0.018
South of Austral F.Z.									
elt29	-28.2	211.0	311.0	162.0	-69.0	25.1	-94.9	25.9	0.008
pol6702	-34.8	214.0	16.0	160.0	-131.2	25.1	-95.5	-35.7	0.008
c0905	-35.5	214.1	15.0	160.0	-129.6	25.1	-95.6	-34.0	0.008
Subtotal									0.042
Seafloor Created by Pacific-Aluk Spreading									
West of V F.Z. and East of Heezen F.Z.									
elt20	-43.8	209.6	53.0	250.0	-121.4	25.1	-118.3	-3.1	0.007
c1212	-43.5	208.3	72.0	250.0	-144.4	20.2	-118.5	-25.9	0.012
v3601	-43.9	207.0	23.0	250.0	-92.1	20.2	-118.3	26.2	0.012
Subtotal									0.031
Seafloor Created by Pacific-Bellingshausen Spreading									
West of Heezen F.Z. and East of Udintsev F.Z.									
end.a409†	-45.2	198.4	45.0	212.0	-131.2	25.1	-113.1	-18.0	0.008
v3602.a	-45.6	197.8	33.0	212.0	-119.7	14.0	-113.1	-6.6	0.025
v3602.b	-46.2	196.9	35.0	213.0	-121.5	10.4	-113.2	-8.3	0.046
elt33	-47.6	195.9	30.0	213.0	-116.8	10.4	-112.9	-3.9	0.046
West of Udintsev F.Z.									
end.a408n†	-48.6	190.1	25.0	213.0	-112.4	25.1	-113.4	1.0	0.008
elt19	-48.2	190.0	38.0	213.0	-125.1	14.0	-113.6	-11.5	0.025
kh6804-c	-48.3	189.9	15.0	213.0	-102.2	20.2	-113.6	11.4	0.012
elt25	-49.3	187.3	43.0	213.0	-130.6	14.0	-113.7	-16.9	0.025
end.odf6†	-49.5	186.9	7.0	213.0	-94.8	25.1	-113.7	18.9	0.008
end.v16†	-50.1	185.3	48.0	214.0	-135.7	25.1	-113.9	-21.8	0.008
um66-b	-50.1	185.2	29.0	214.0	-116.6	20.2	-113.9	-2.7	0.012
Subtotal									0.223
Seafloor Created by Pacific-Antarctica Spreading									
East of Endeavor F.Z.									
end.odf8†	-52.1	184.8	51.0	242.0	-131.3	25.1	-115.5	-15.7	0.008
end.w†	-52.2	184.3	85.0	243.0	-165.2	25.1	-115.6	-49.6	0.008
um6402-b	-52.8	182.6	16.0	244.0	-96.3	10.4	-115.5	19.2	0.045
end.t	-52.8	182.4	24.0	244.0	-104.4	10.4	-115.6	11.1	0.045
gecs-gmv	-52.9	182.2	24.0	244.0	-104.6	10.4	-115.5	10.9	0.045
mons06ar.a	-53.0	181.4	20.0	245.0	-100.5	14.0	-115.6	15.1	0.025
elt43	-53.0	181.3	344.0	245.0	-64.5	20.2	-115.6	51.1	0.012
elt27	-53.5	178.8	50.0	247.0	-130.5	25.1	-115.7	-14.9	0.008
West of Endeavor F.Z. and East of XII F.Z.									
end.k	-54.9	175.9	70.0	250.0	-151.2	25.1	-115.3	-35.9	0.008
elt52	-55.7	174.9	10.0	251.0	-91.7	10.4	-115.0	23.3	0.045
West of XII F.Z. and East of XIII F.Z.									
end.q	-56.1	173.7	37.0	253.0	-118.7	10.4	-114.9	-3.8	0.045
end.b	-56.1	172.9	14.0	253.0	-95.8	14.0	-115.0	19.2	0.025
end.v†	-56.1	171.8	17.0	254.0	-98.7	25.1	-115.1	16.4	0.008
end.a707†	-56.3	171.6	36.0	254.0	-117.9	25.1	-115.0	-2.9	0.008
West of XIII F.Z.									
end.n	-57.1	169.9	25.0	256.0	-107.3	25.1	-114.7	7.4	0.008
elt34	-57.2	169.9	20.0	256.0	-102.3	14.0	-114.6	12.3	0.025
mons06ar.b	-57.3	169.2	47.0	257.0	-129.0	20.2	-114.6	-14.4	0.012
end.r	-57.4	168.0	26.0	258.0	-108.4	20.2	-114.7	6.3	0.012
cp7808.a	-57.5	166.7	29.0	259.0	-111.7	14.0	-114.7	3.0	0.025
cp7808.b	-57.5	166.5	45.0	259.0	-127.8	14.0	-114.7	-13.0	0.025
Subtotal									0.442
Total									3.005

The apparent effective inclination, e_a, was obtained from the phase shift $\Delta\theta$ using eq. (1), where $\Delta\theta$ is the quantity opposite to Schouten & Cande's (1976) θ. The model effective inclination, e_m, was calculated from the best-fitting values for palaeomagnetic pole latitude, longitude, and anomalous skewness (Petronotis *et al.* 1992). Although ordinary palaeomagnetic inclinations are defined only between $-90°$ and $+90°$, effective remanent inclinations of the seafloor can be usefully defined between $-180°$ and $+180°$ (Gordon & Cox 1980). Values between $-90°$ and $+90°$ correspond to magnetic vectors with a positive horizontal component in the direction in which seafloor age decreases, and other values correspond to magnetic vectors with a positive horizontal component in the direction in which seafloor age increases (Gordon & Cox 1980). '†' indicates profiles digitized from Christoffel & Falconer (1972). The nn, ne, na, ee, ea, and aa elements of the error covariance matrix are respectively 0.577, −0.304, 0.717, 2.584, 0.396, and 3.567 in units of (great-circle) degrees squared, where 'n' denotes north, 'e' denotes east, and 'a' denotes anomalous skewness.

approximation. He shows that when large fluctuations in intensity of magnetization are permitted in his models, the direction of magnetization is poorly constrained. His results indicate that uncertainties in seamount poles are large, far larger than illustrated for the four examples shown in Fig. 19.

These arguments, however, do not imply that skewness poles suffer from this limitation. Our new pole is determined from more than 100 crossings of magnetic anomaly 32 distributed over more than 12 000 km, whereas a typical seamount survey used to determine a seamount pole typically incorporates a half dozen or so crossings over distances typically less than ~50 km. A seamount pole is subject to uncertainties that are strongly correlated between distinct profiles. A crossing of anomaly 32 may be just as susceptible as a seamount crossing to fluctuations in the magnetic intensity of the source material. Because of the wide spacing between the profiles we use, however, there is little reason to expect these fluctuations to be correlated from profile to profile. These fluctuations, then, are expected merely to increase the dispersion of apparent effective inclination about the best-fitting model, which is already fully reflected in our confidence limits.

Pacific apparent polar wander

The new chron 32 (73 Ma) palaeomagnetic pole differs significantly from and lies 7.8 great-circle degrees to the ENE of a previously estimated coeval (72 Ma) pole for the Pacific plate (Fig. 20) (Sager & Pringle 1988). The longitude of this previously estimated pole is strongly influenced by the inclusion of five seamount poles, and seems unlikely to be as reliable as the longitude of the new pole. The new 73 Ma pole lies even farther from the published 82 Ma pole (Gordon 1983; Sager & Pringle 1988) than does the previously estimated 72 Ma pole. Thus, insofar as the 82 Ma pole is accurate, it indicates fast APW from 82 to 73 Ma. However, the published 82 Ma pole relies mainly on seamount poles and is currently open to question. Unpublished analyses of the skewness of Pacific plate anomalies 33n (74–79 Ma) and 33r (79–83 Ma) give poles that are similar to the chron 32 pole that we present here and thus indicate little, if any, APW between 82 and 73 Ma (Vasas, Gordon & Petronotis, in preparation). These unpublished results agree better with basalt colatitude data (Cox & Gordon 1984) than do the seamount poles. In particular, new palaeolatitude

data from Detroit seamount agree decisively better with our unpublished skewness poles than with the seamount poles (Tarduno & Cottrell 1997).

Comparison with Pacific plate motion relative to hotspots

It is well established that the Hawaiian hotspot shifted $\sim 8^\circ$ southwards relative to the palaeomagnetic axis during Cenozoic times (Kono 1980; Gordon & Cape 1981; Gordon 1982, 1983; Sager 1983, 1987). In Fig. 21 we show a compilation of the northward-motion data of the Pacific plate that were used in these studies.

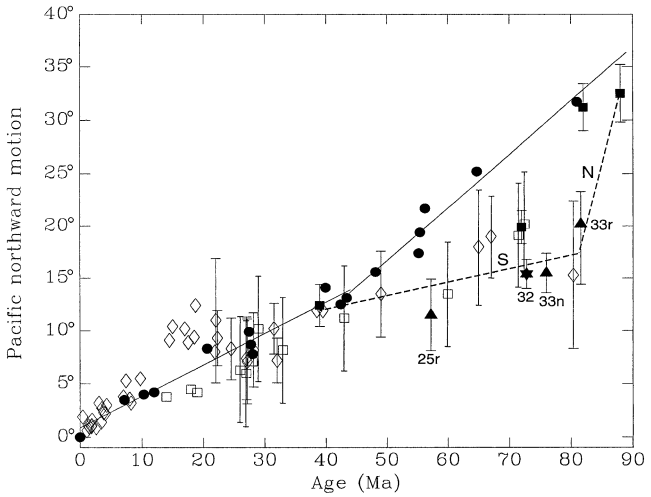

Figure 21. Northward motion of the Pacific plate inferred from dated seamounts and islands of the Hawaiian–Emperor chain (solid circles), palaeomagnetic poles (solid squares, solid triangles, and star), palaeomagnetically determined palaeolatitudes from azimuthally unoriented cores (open diamonds), and sediment facies that record the passage of the plate through the equatorial zone (open squares). Solid squares show northward motion inferred from palaeopoles determined entirely or mainly from seamount magnetism. The star shows the northward motion inferred from the anomaly 32 skewness pole determined in this paper. Solid triangles show the results from other palaeopoles determined entirely from skewness data. The northward motion of a dated volcano (circles) is the present latitude of the volcano minus the present latitude of Kilauea (19.6°N). The northward motion of a palaeomagnetic datum is the present latitude of either a drill site (if the datum consists of inclination-only data from a single site) or a reference site along the Hawaiian–Emperor chain (if the datum is a palaeomagnetic pole) minus the palaeolatitude of that site. Error bars are 1-D 95 per cent confidence limits. Straight lines (solid) were fit to two subsets of Hawaiian–Emperor age dates: the young segment extends to 43 Ma and is best fit by a line with a slope of $0.30^\circ \pm 0.04^\circ$ Myr^{-1} (95 per cent confidence limits) and an intercept of $0.87^\circ \pm 1.14^\circ$ (95 per cent confidence limits), and the old segment extends from 43 to 90 Ma and is best fit by a line with a slope of $0.50^\circ \pm 0.09^\circ$ Myr^{-1} (95 per cent confidence limits) and an intercept of $-8.53^\circ \pm 5.1^\circ$ (95 per cent confidence limits). The two dashed lines show an interpretation of the palaeomagnetically determined northward motion discussed in the text. Figure modified from Gordon & Cape (1981) and Petronotis *et al.* (1994). Other sources of data include Kono (1980), Suárez & Molnar (1980), Prince *et al.* (1980), Epp *et al.* (1983), Sager (1987), Sager & Pringle (1988), and Vasas *et al.* (in preparation).

For almost all ages greater than 39 Ma, the Pacific plate has had greater northward motion relative to the hotspots than it has had relative to the spin axis (Fig. 21). The northward motion suggested by the new 73 Ma pole is slightly less than that suggested by coeval sediment facies data, but is within the $\sim 5^\circ$ uncertainty of the latter (Fig. 19) (Gordon & Cape 1981). The consistency of the chron 25r and chron 32 palaeomagnetic poles with the equatorial sediment facies data over the earlier time interval excludes an explanation depending on the presence of large non-dipole components of the palaeomagnetic field to explain the inferred southward drift of the Hawaiian hotspot.

Most of the data in Fig. 21, in particular the skewness data, may be best explained by two episodes of latitudinal drift of the Hawaiian hotspot. If one accepts the 88 Ma pole determined from seamounts, but rejects the 82 Ma poles determined from seamounts, the earlier episode, which corresponds to the dashed-line segment labelled 'N' in Fig. 21, began near 88 Ma, ended near 81 Ma, and resulted in rapid northward motion of the Hawaiian hotspot ($\sim 11^\circ$ in ~ 7 Myr for a drift rate of ~ 170 mm yr^{-1}). The later episode, which corresponds to the dashed-line segment labelled 'S' in Fig. 21, began near 81 Ma, ended near 39 Ma, and resulted in southward motion of the Hawaiian hotspot ($\sim 14^\circ$ in ~ 42 Myr for a drift rate of ~ 40 mm yr^{-1}). In both cases, the timing and magnitude of drift is open to question because of the critical role of the 88 and the 39 Ma palaeomagnetic poles, which were determined mainly from seamount poles. The result that remains firm, however, is that both the 57 and 73 Ma poles show distinctly less northward motion than indicated by the present latitude of coeval volcanoes on the Emperor chain: 9° less northward motion for the 57 Ma pole and 13° less for the 73 Ma pole.

The shift of the palaeomagnetic pole relative to the Pacific hotspots is fully specified in Fig. 22, in which the 57 and 73 Ma poles determined from skewness are reconstructed with the Pacific plate relative to the hotspots. The rotation for 57 Ma, 37.88° about 55.47°N, 71.16°W, and the rotation for 73 Ma, 43.65° about 48.57°N, 77.22°W, were interpolated from the rotations given in Table 2. The position of the palaeomagnetic axis relative to the hotspots at 73 Ma differs significantly from that at 57 Ma. The reconstructed 57 Ma pole lies 9°, and the reconstructed 73 Ma pole lies 16°, from the north pole of the coordinate system fixed with respect to the Pacific hotspots. The 16° distance between the 73 Ma pole and the north pole of the hotspot reference frame is larger than the 13° southward motion of the Hawaiian hotspot since 73 Ma inferred above, because the 16° distance incorporates differences in both declination and inclination, as seen from the location on the Pacific plate that was above the hotspot at 73 Ma (47.9°N, 169.0°E in our rotation model), whereas the 13° distance only includes the effect of the difference in inclination.

Also shown in Fig. 22 are mean continental palaeomagnetic poles reconstructed relative to hotspots in the African and Indian oceans, as determined by Besse & Courtillot (1991) from 20-Myr-long age intervals centred on 50, 60, 70, and 80 Ma. Neither the Pacific nor the Indo–Atlantic set of poles incorporates uncertainties in the reconstructions of the plates relative to the hotspots; no published method has shown how to estimate these uncertainties correctly. The Pacific hotspot 57 Ma pole differs insignificantly from the Indo–Atlantic 60 Ma pole, indicating consistency with the assumption of the Pacific hotspots being stationary relative to the Indo–Atlantic hotspots

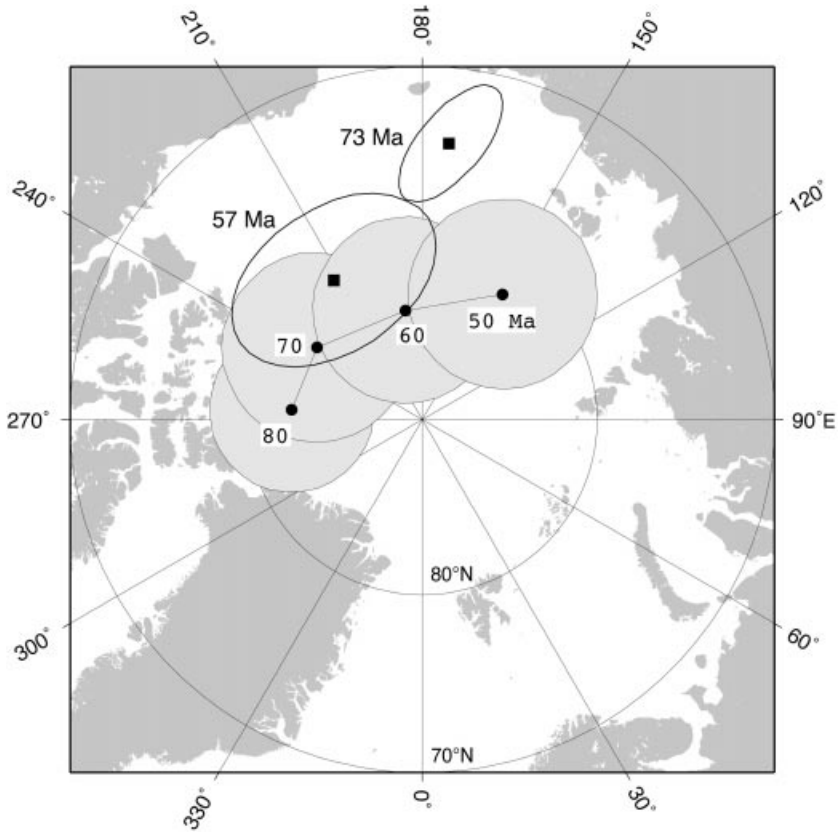

Figure 22. Pacific (57 and 73 Ma) and non-Pacific (50, 60, 70, and 80 Ma; Besse & Courtillot 1991) palaeomagnetic poles positioned in a fixed hotspot reference frame. Meridians and parallels are shown every 10° (stereographic projection).

Table 2. Rotation of the Pacific plate relative to the hotspots

Age (Myr)	Latitude °N	Longitude °E	Ω (degrees)
3	61.000	−95.000	3.000
5	61.700	−82.800	4.800
20	68.000	−75.000	19.000
43	64.200	−58.400	32.800
65	51.168	−75.185	41.240
80	46.497	−78.694	45.836
95	43.986	−76.299	62.616

Each rotation reconstructs the Pacific plate relative to the hotspots from its present position to its position at the stated age. From R. G. Gordon, unpublished reconstructions.

for the past 60 Myr. Within the joint uncertainties of the 57 Ma Pacific hotspot pole and 60 Ma Indo–Atlantic hotspot pole, however, differences of up to ∼10° are possible. In any event, the agreement between the poles, both of which are offset from the present spin axis (i.e. the north pole of the hotspot reference frame) in a similar direction, suggests that the Pacific and Indo–Atlantic hotspots have had a common component of motion relative to the spin axis, as might be expected as a consequence of true polar wander.

In contrast, the 73 Ma pole for the Pacific hotspots differs significantly from the 70 and 80 Ma poles for the Indo–Atlantic hotspots (Fig. 22), and lies respectively 13.8° and 17.6° from the two poles. There are many possible explanations for this difference, including the following: (1) a large bias, including that caused by a large non-dipole component of the field, in one or more of the poles; (2) substantial motion of Pacific hotspots relative to Indo–Atlantic hotspots between 57 and 73 Ma; and (3) substantial errors in the reconstructions from ∼57 to ∼73 Ma of the Pacific plate, the Indo–Atlantic plates, or both relative to the hotspots. It would be possible to distinguish better between some of these explanations if there were more high-resolution Pacific palaeomagnetic poles determined from skewness, in particular so that the pattern of APW of Pacific hotspots was better established.

CONCLUSIONS

Numerical experiments on the variation of anomalous skewness over the range of observed spreading rates indicate little, if any, dependence on spreading half-rate over the range of ∼25 to ∼90 mm yr^{-1}. The new chron 32 pole is consistent with palaeocolatitudes inferred from the palaeomagnetism of igneous rocks recovered in vertical, azimuthally unoriented cores and from palaeoequatorial sediment facies, but differs significantly from seamount poles. We attribute the difference to unmodelled errors in the seamount poles, mainly in the declinations. Comparison with the northward motion inferred from dated volcanoes along the Hawaiian–Emperor seamount

chain indicates 13° of southward motion of the Hawaiian hotspot since 73 Ma. When the pole is reconstructed with the Pacific plate relative to the Pacific hotspots, it differs by 14°–18° from the position of the pole relative to the Indo–Atlantic hotspots, which has several possible explanations including bias in one or more of the palaeomagnetic poles, motion between Pacific and Indo–Atlantic hotspots, and errors in plate reconstructions relative to the hotspots.

ACKNOWLEDGMENTS

KEP dedicates this paper to her son Alexander. We thank Gary Acton and Stephen Vasas for their contributions at various stages of this work, and Steve Cande and Will Sager for helpful reviews. This work was supported by National Science Foundation grants EAR-9205875 (KEP), EAR-9632858, and EAR-9796110 (RGG).

REFERENCES

Acton, G.D. & Gordon, R.G., 1991. A 65 Ma palaeomagnetic pole for the Pacific Plate from the skewness of magnetic anomalies 27r-31, *Geophys. J. Int.,* **106,** 407–420.

Acton, G.D. & Gordon, R.G., 1994. Paleomagnetic tests of Pacific plate reconstructions and implications for motion between hotspots, *Science,* **263,** 1246–1254.

Atwater, T. & Severinghaus, J., 1989. Tectonic maps of the northeast Pacific, in *The Eastern Pacific Ocean and Hawaii, The Geology of North America N,* pp. 15–20, eds Winterer, E.L., Hussong, D.M. & Decker, R.W., Geological Society of America, Boulder.

Besse, J. & Courtillot, V., 1991. Revised and synthetic apparent polar wander paths of the African, Eurasian, North American and Indian Plates, and true polar wander since 200 Ma, *J. geophys. Res.,* **96,** 4029–4050.

Cande, S.C., 1976. A palaeomagnetic pole from Late Cretaceous marine magnetic anomalies in the Pacific, *Geophys. J. R. astr. Soc.,* **44,** 547–566.

Cande, S.C., 1978. Anomalous behavior of the paleomagnetic field inferred from the skewness of anomalies 33 and 34, *Earth planet. Sci. Lett.,* **40,** 275–286.

Cande, S.C. & Kent, D.V., 1976. Constraints imposed by the shape of marine magnetic anomalies on the magnetic source, *J. geophys. Res.,* **81,** 4157–4162.

Cande, S.C. & Kent, D.V., 1992. A new geomagnetic polarity time scale for the Late Cretaceous and Cenozoic, *J. geophys. Res.,* **97,** 13 917–13 951.

Cande, S.C. & Kristoffersen, Y., 1977. Late Cretaceous magnetic anomalies in the North Atlantic, *Earth planet. Sci. Lett.,* **35,** 215–224.

Cande, S.C., Herron, E.M. & Hall, B.R. 1982. The early Cenozoic history of the southeast Pacific, *Earth planet. Sci. Lett.,* **57,** 63–74.

Christoffel, D.A. & Falconer, R.K.H., 1972. Marine magnetic anomalies in the South-west Pacific Ocean and the identification of new tectonic features, in *Antarctic Oceanology II: The Australian–New Zealand Sector, Antarctic Res. Ser. 19,* pp. 197–209, ed. Hayes, D.E., AGU, Washington, DC.

Cox, A. & Gordon, R.G., 1984. Paleolatitudes determined from paleomagnetic data from vertical cores, *Rev. Geophys. Space Phys.,* **22,** 47–72.

Dyment, J., Cande, S.C. & Arkani-Hamed, J., 1994. Skewness of marine magnetic anomalies created between 85 and 40 Ma in the Indian Ocean, *J. geophys. Res.,* **99,** 21 121–24 134.

Engebretson, D.C., Cox, A. & Gordon, R.G., 1984. Relative motions between oceanic plates of the Pacific basin, *J. geophys. Res.,* **89,** 10 291–10 310.

Epp, D., Sager, W.W., Theyer, F. & Hammond, S.R., 1983. Hotspot-spin axis motion or magnetic far-sided effect, *Nature,* **303,** 318–320.

Gordon, R.G., 1982. The late Maastrichtian palaeomagnetic pole of the Pacific plate, *Geophys. J. R. astr. Soc.,* **70,** 129–140.

Gordon, R.G., 1983. Late Cretaceous apparent polar wander of the Pacific plate: Evidence for a rapid shift of the Pacific hotspots with respect to the spin axis, *Geophys. Res. Lett.,* **10,** 709–712.

Gordon, R.G. & Cape, C.D., 1981. Cenozoic latitudinal shift of the Hawaiian hotspot and its implications for true polar wander, *Earth planet. Sci. Lett.,* **55,** 37–47.

Gordon, R.G. & Cox, A., 1980. Calculating palaeomagnetic poles for oceanic plates, *Geophys. J. R. astr. Soc.,* **63,** 619–640.

Grim, P.J. & Erickson, B.H., 1969. Fracture zones and magnetic anomalies south of the Aleutian Trench, *J. geophys. Res.,* **74,** 1488–1494.

Hildebrand, J.A. & Parker, R.L. 1987. Paleomagnetism of Cretaceous Pacific seamounts revisited, *J. geophys. Res.,* **92,** 12 695–12 712.

Kono, M., 1980. Paleomagnetism of DSDP leg 55 basalts and implications for the tectonics of the Pacific plate, *Init. Rep. Deep Sea Drill. Proj.,* **55,** 737–752.

Lonsdale, P., 1988. Paleogene history of the Kula plate: Offshore evidence and onshore implications, *Geol. Soc. Am. Bull.,* **100,** 733–754.

Macdonald, K.C., Haymon, R.M., Miller, S.P., Sempere, J.-C. & Fox, P.J., 1988. Deep-Tow and Sea Beam studies of dueling propagating ridges on the East Pacific Rise near 20°40′S, *J. geophys. Res.,* **93,** 2875–2898.

Mayes, C.L., Lawver, L.A. & Sandwell, D.T., 1990. Tectonic history and new isochron chart of the South Pacific, *J. geophys. Res.,* **95,** 8543–8567.

Parker, R.L., 1991. A theory of ideal bodies for seamount magnetism, *J. geophys. Res.,* **96,** 16 101–16 112.

Petronotis, K.E. & Gordon, R.G., 1989. Age dependence of skewness of magnetic anomalies above seafloor formed at the Pacific-Kula spreading center, *Geophys. Res. Lett.,* **16,** 315–318.

Petronotis, K.E., Gordon R.G. & Acton, G.D., 1992. Determining palaeomagnetic poles and anomalous skewness from marine magnetic anomaly skewness data from a single plate, *Geophys. J. Int.,* **109,** 209–224.

Petronotis, K.E., Gordon, R.G. & Acton, G.D., 1994. A 57 Ma Pacific plate paleomagnetic pole determined from a skewness analysis of crossings of marine magnetic anomaly 25r, *Geophys. J. Int.,* **118,** 529–554.

Prince, R.A., Heath, G.R. & Kominz, M., 1980. Paleomagnetic studies of central North Pacific sediment cores: stratigraphy, sedimentation rates, and the origin of magnetic instability, *Geol. Soc. Am. Bull.,* **91,** 1789–1835.

Rea, D.K. & Dixon, J.M., 1983. Late Cretaceous and Paleogene tectonic evolution of the North Pacific Ocean, *Earth planet. Sci. Lett.,* **65,** 145–166.

Roest, W.R., Arkani-Hamed, J. & Verhoef, J., 1992. The seafloor spreading rate dependence of the anomalous skewness of marine magnetic anomalies, *Geophys. J. Int.,* **109,** 653–669.

Rosa, J.C.C. & Molnar, P., 1988. Uncertainties in reconstructions of the Pacific, Farallon, Vancouver, and Kula plates and constraints on the rigidity of the Pacific and Farallon (and Vancouver) plates between 72 and 35 Ma, *J. Geophys. Res.,* **93,** 2997–3008.

Sager, W.W., 1983. A late Eocene paleomagnetic pole for the Pacific plate, *Earth planet. Sci. Lett.,* **63,** 408–422.

Sager, W.W., 1987. Late Eocene and Maastrichtian paleomagnetic poles for the Pacific plate: implications for the validity of seamount paleomagnetic data, *Tectonophysics,* **144,** 301–314.

Sager, W.W. & Pringle, M.S., 1988. Mid-Cretaceous to early Tertiary apparent polar wander path of the Pacific plate, *J. geophys. Res.,* **93,** 11 753–11 771.

Schouten, H. & Cande, S.C., 1976. Palaeomagnetic poles from marine magnetic anomalies, *Geophys. J. R. astr. Soc.,* **44,** 567–575.

Schouten, H. & McCamy, K., 1972. Filtering marine magnetic anomalies, *J. geophys. Res.,* **77,** 7089–7099.

Stock, J. & Molnar, P., 1982. Uncertainties in the relative positions of the Australia, Antarctica, Lord Howe, and Pacific plates since the Late Cretaceous, *J. geophys. Res.,* **87,** 4697–4714.

Stock, J. & Molnar, P., 1987. Revised history of early Tertiary plate motion in the south-east Pacific, *Nature,* **325,** 495–499.

Suárez, G. & Molnar, P., 1980. Paleomagnetic data and pelagic sediment facies and the motion of the Pacific plate relative to the spin axis since the Late Cretaceous, *J. geophys. Res.,* **85,** 5257–5280.

Tarduno, J.A. & Cottrell, R.D., 1997. Paleomagnetic evidence for motion of the Hawaiian hotspot during formation of the Emperor seamounts, *Earth planet. Sci. Lett.,* **153,** 171–180.

Weissel, J.K. & Hayes, D.E., 1972. Magnetic anomalies in the southeast Indian Ocean, in *Antarctic Oceanology II: The Australian–New Zealand Sector, Antarctic Res. Ser. 19,* pp. 165–196, ed. Hayes, D.E., AGU, Washington, DC.